

# Sources, concentrations, and seasonal variations of VOC and aerosol particles in downtown Munich in 2023/24

Yanxia Li<sup>1</sup>, Hengheng Zhang<sup>1,a</sup>, Xuefeng Shi<sup>1</sup>, Yaowei Li<sup>2,b</sup>, Sophie Abou-Rizk<sup>2</sup>, Jessica B. Smith<sup>2</sup>, Zhaojin An<sup>2,c</sup>, Adrian Wenzel<sup>3</sup>, Junwei Song<sup>4</sup>, Thomas Leisner<sup>1,5</sup>, Frank Keutsch<sup>2</sup>, Jia Chen<sup>3</sup>, and Harald Saathoff<sup>1</sup>

<sup>1</sup>Institute of Meteorology and Climate Research-Atmospheric Aerosol Research, Karlsruhe Institute of Technology, 76344 Eggenstein-Leopoldshafen, Germany

<sup>2</sup>Paulson School of Engineering and Applied Sciences, Harvard University, Cambridge, MA 02138, USA

<sup>3</sup>Environmental Sensing and Modeling, Technical University of Munich (TUM), Munich, Germany

<sup>4</sup>Irceylon, Université Claude Bernard Lyon 1, CNRS, UMR 5256, Villeurbanne, 69100, France

<sup>5</sup>Institute of Environmental Physics, Heidelberg University, 69120 Heidelberg, Germany

<sup>a</sup>now at: Research Institute for Applied Mechanics, Kyushu University, Fukuoka, Japan

<sup>b</sup>now at: Department of Earth, Atmospheric, and Planetary Sciences, Massachusetts Institute of Technology, Cambridge, MA 02139, USA

<sup>c</sup>now at: School of Environment, Tsinghua University, 10084, Beijing China

*Corresponding authors: Yanxia Li (yanxia.li@kit.edu) and Harald Saathoff (Harald.Saathoff@kit.edu)*

**Abstract.** Little is known about molecular composition and sources of air pollution in Germany's third largest city, Munich. Therefore, we investigated sources, concentrations, and seasonal variations of volatile organic compounds (VOC), semi-volatile organic aerosol (SVOA), and organic aerosol (OA) in an urban street canyon in Munich utilizing online mass spectrometry and positive matrix factorization (PMF). Organic aerosol concentrations were higher in summer ( $4.3 \pm 2.9 \mu\text{g m}^{-3}$ ) than late winter ( $3.3 \pm 1.7 \mu\text{g m}^{-3}$ ), consistent with enhanced photochemical reactions, while nitrate exhibited the opposite trend with elevated concentrations in winter ( $4.5 \pm 3.2 \mu\text{g m}^{-3}$ ) compared to summer ( $0.3 \pm 0.2 \mu\text{g m}^{-3}$ ). During summer heat, photochemistry is associated with the formation of low-volatile oxygenated OA ( $33 \pm 20\%$ ), while aged biomass burning organic aerosol (BBOA) ( $25 \pm 21\%$ ) associated with barbecue activities and biogenic OA ( $22 \pm 14\%$ ) linked to nocturnal monoterpene chemistry further shape aerosol composition. The colder seasons are characterized by combustion-derived aerosols (Winter: fresh BBOA  $13 \pm 9\%$ , aged  $36 \pm 12\%$ ; Spring: fresh  $27 \pm 17\%$ , aged  $37 \pm 19\%$ ), whose dynamics are driven mainly by anthropogenic activity patterns. Traffic contributed at this urban kerbside relatively little to aerosol mass (5-9 %) but more to VOC (22-35%). Our findings point to potential strategies to improve air quality e.g. by reducing monoterpene emissions by urban vegetation management as well as reducing biomass burning including barbecue emissions, which are attributed to a substantial fraction of aerosol particles and precursor gases of secondary organic aerosol throughout the seasons.

## 1. Introduction

Volatile organic compounds (VOC) and organic aerosols (OA) are major components of urban air pollution, contributing to the formation of secondary pollutants like ozone and secondary organic aerosol (SOA), which pose significant risks to air quality, climate, and human health (Wu et al., 2020; Nault et al., 2021; IPCC, 2023). Moreover, different weather conditions and seasons influence the dispersion, deposition, and transformation of these pollutants (Crippa et al., 2013; Debevec et al., 2021; Stirnberg et al., 2021). Identifying SOA sources is

40 crucial for reducing complex observational datasets to key real-world contributors, enabling timely air quality  
41 management, policy evaluation, and accurate air pollution forecasting (Chen et al., 2022a). However, pinpointing  
42 the sources of SOA is particularly challenging due to its composition as a highly complex mixture of largely  
43 unidentified compounds, coupled with the complicated and multistep transformation processes of VOC into SOA  
44 (Daellenbach et al., 2019).

45 The high-resolution time-of-flight Aerodyne aerosol mass spectrometer (HR-TOF-AMS, Aerodyne Research Inc.,  
46 Billerica, MA, USA) quipped with a PM<sub>2.5</sub> aerodynamic lens is used for the online characterization of non-  
47 refractory PM<sub>2.5</sub>. Positive matrix factorization (PMF) analysis of AMS datasets can quantitatively resolve major  
48 primary organic aerosol (POA) sources, including traffic-related hydrocarbon-like organic aerosol (HOA) and  
49 biomass burning organic aerosol (BBOA) (Chakraborty et al., 2017; Lalchandani et al., 2021). However, AMS  
50 datasets cannot specify sources for secondary organic aerosol (SOA) due to significant fragmentation from  
51 thermal volatilization (~600°C) and harsh electron impact ionization (~70 eV) (Qi et al., 2020; Kumar et al.,  
52 2022). Additionally, without information on VOC as SOA precursors, it is difficult to attribute SOA factors (e.g.,  
53 semi-volatile oxygenated OA (SV-OOA) and low-volatility oxygenated OA (LV-OOA)) to specific sources or  
54 formation mechanisms using AMS-PMF analysis (Song et al., 2024). Proton transfer reaction time-of-flight mass  
55 spectrometry (PTR-TOF-MS) is a useful tool to identify the sources of VOC and oxygenated VOC (OVOC), and  
56 in elucidating their contributions to the SOA formation (Wang et al., 2020a; Pfannerstill et al., 2019). Furthermore,  
57 the CHARON-PTR-MS (Chemical Analysis of Aerosol Online Particle Inlet coupled to a PTR-TOF-MS) is a  
58 continuous measurement technique capable of providing molecular-level chemical characterization and time-  
59 resolved quantification of semi-volatile organic aerosol components (Eichler et al., 2015; Muller et al., 2017; Piel  
60 et al., 2019). CHARON-PTR-MS enhances the detection of detailed SOA chemical composition data by  
61 minimizing thermal decomposition and ionization-induced fragmentation compared to AMS employing high-  
62 temperature vaporization and electron-impact ionization (Gkatzelis et al., 2018b; Leglise et al., 2019). This is  
63 achieved through lower thermal stress during particle evaporation at reduced pressure and softer chemical  
64 ionization via proton-transfer reactions, which better preserves molecular information.

65 Huang et al. (2019) found that in the city of Stuttgart (southwest Germany) SOA from VOC oxidation dominated  
66 the organic aerosol burden, with primary sources like traffic contributing less, while residential wood burning  
67 became particularly important during winter in residential areas. A study in downtown Karlsruhe (southwest  
68 Germany) demonstrated that secondary oxygenated OA comprised over 60-75% of total OA throughout the year,  
69 with primary traffic-related OA showing seasonal variations and wood combustion becoming more significant  
70 during cold periods under stagnant meteorological conditions (Song et al., 2022). A Europe-wide analysis revealed  
71 that oxygenated OA (secondary formation) accounted for an average of 71% of submicron OA mass across 22  
72 sites, with solid fuel/biomass burning contributing 16% and primary urban sources (traffic, cooking) typically less  
73 than 10-15% (Chen et al., 2022b). These findings underscore the necessity for site-specific OA and VOC source  
74 apportionment studies in major European cities such as Munich in southern Germany. Although secondary  
75 formation processes consistently dominate regional OA burdens, the underlying VOC precursors, and primary  
76 emission contributions exhibit substantial spatial and temporal variability.

77 Munich, the capital of Bavaria, Germany, is a major cultural and economic center with a population of 1.5 million  
78 as of 2023, making it the third-largest city in Germany. It has a population density of 4,700 people per square  
79 kilometers (München, 2023). Despite significant progress in air quality regulations, Munich still struggles with

80 aerosol pollution. Identifying the sources of VOC and particulate matter is crucial for improving air quality in  
81 Munich. However, there have been only a limited number of studies characterizing aerosols in Munich. Schnelle-  
82 Kreis J. et al. (2001) collected filters from three traffic-dominated sites and one additional site located on the  
83 northern outskirts of Munich, approximately 1 km from the city center, between 1996 and 1998. Using HPLC  
84 analysis, they found that 40% of polycyclic aromatic hydrocarbons (PAHs) were associated with fine particles.  
85 Schäfer et al. (2011) monitored air pollution across Munich and its outskirts, employing long-term as well as  
86 campaign-based monitoring stations from LfU (Bayerisches Landesamt Für Umwelt), Meteorological Institute  
87 of the Ludwig-Maximilians-University Munich (MIM), and IMK-IFU (e.g., Maisach) covering traffic-related  
88 (e.g., Lothstraße, Stachus, Luise-KiesselbachPlatz), urban (MIM), and suburban (Johanneskirchen) sites, during  
89 campaigns in late spring (10th-30th May 2003) and winter (27th November-15th December 2003). They found  
90 higher particle mass concentrations at the urban site compared to rural areas, especially in winter, with no  
91 significant differences in major ionic composition between the sites (Schäfer et al., 2011). Qadir et al. (2013)  
92 identified traffic, cooking, solid fuel combustion, and mixed aerosols (from tobacco smoke, cooking, and wood  
93 combustion) as the primary sources of aerosols at Lothstraße in Munich during the winter periods of October 2006  
94 to February 2007 and October 2009 to February 2010. Schnell (2014) identified biomass burning aerosol as the  
95 dominant aerosol type at the rural site of Maisach and the urban site of MIM during the winter seasons from 2007  
96 to 2010. Recently, a study on aerosol emissions from Munich Airport showed its impact in the outskirts of Munich,  
97 especially for ultrafine particles (UFPs) (Seidler et al., 2024). Despite these previous studies, we still have limited  
98 understanding of the main sources of VOC and OA through concurrent online measurements, their typical  
99 concentration levels across seasons, and their seasonal variations in molecular composition in Munich. It remains  
100 unclear how much anthropogenic and biogenic sources contribute to organic aerosol in Munich and what is the  
101 fraction of biomass burning aerosol originates from residential wood combustion versus barbecue activities.  
102 Therefore, we examined in this study the seasonal variability of OA and VOC chemical composition at a molecular  
103 level in a street canyon (Theresienstrasse 39) in downtown Munich, aiming to elucidate the contribution of  
104 different sources to major VOC, SVOA, and total OA concentrations. The PM<sub>2.5</sub> concentrations at the  
105 Theresienstrasse were measured using a FIDAS 200 optical particle spectrometer (Palas GmbH, Germany) and  
106 are comparable to those observed at the regulatory monitoring station Munich/Stachus of LfU. For 2023, the  
107 annual average PM<sub>2.5</sub> concentration at the reference station was  $9.3 \pm 6.2 \mu\text{g m}^{-3}$ , with August showing  $8.7 \pm 5.7$   
108  $\mu\text{g m}^{-3}$ , compared to our measured value of  $6.7 \pm 3.7 \mu\text{g m}^{-3}$ . In 2024, the annual average at the reference station  
109 was  $8.7 \pm 6.6 \mu\text{g m}^{-3}$ , with March averaging  $9.0 \pm 9.9 \mu\text{g m}^{-3}$ , while our March measurements yielded  $8.7 \pm 9.2$   
110  $\mu\text{g m}^{-3}$ . Both measurement periods demonstrated strong correlations ( $R=0.8$ ) (Figure S1). The close agreement  
111 between our measurements and the official monitoring data, combined with the high correlation coefficients,  
112 validates the representativeness of our sampling location for characterizing the urban downtown atmosphere in  
113 Munich. Please note that this work is linked to the recently established low-cost sensor network in downtown  
114 Munich, monitoring especially O<sub>3</sub>, NO<sub>2</sub>, and PM<sub>2.5</sub> (Wenzel et al., 2025). For our dedicated source apportionment,  
115 we conduct separate statistical analyses on VOC from PTR-TOF-MS, SVOA from CHARON-PTR-MS, and OA  
116 from HR-TOF-AMS to identify the sources of VOC, SVOA, and OA from their chemical fingerprints.

## 117 **2. Methodology**

### 118 **2.1 Measurement location**

119 Field observations were conducted during three meteorological periods: summer (3<sup>rd</sup>-29<sup>th</sup> August 2023), late  
120 winter (1<sup>st</sup>-8<sup>th</sup> March 2024), and spring (9<sup>th</sup>-27<sup>th</sup> March 2024). The separation between winter and spring periods  
121 was based on observed transitions in ambient temperature and chemical composition, including systematic  
122 changes in organic aerosol and nitrate concentrations observed in the time series (Figure 1d and Figure 2),  
123 indicating a shift from colder, nitrate-favored conditions to warmer conditions associated with enhanced  
124 photochemical activity. Spring conditions were characterized by higher solar radiation and an increased relative  
125 contribution of organic aerosol (Figure 1d and Figure 2), reflecting stronger photochemical production. These  
126 periods therefore represent meteorologically and chemically distinct regimes rather than strict calendar-based  
127 seasonal classifications. The sampling site (11°57'E, 48°15'N) was located on a parking lot next to a 30 m tall  
128 building of the Ludwigs-Maximilians-University (LMU) of Munich in a street canyon of Theresienstrasse 39  
129 (Figure S2). The elevation on street level at this location is 520 m a.s.l. The street has several restaurants,  
130 apartment buildings, museums, university workshops, laboratories, and substantial vehicular traffic. The wind  
131 direction at the site in the street canyon predominantly originates from the south and southeast due to a vortex due  
132 to upwind or lee side of the LMU building. At the rooftop of the 30-meter LMU building, it mainly came from  
133 the west and east. Wind speed and direction exhibit minimal variation for the measurement periods (Figure S2).

### 134 **2.2 Instrumentation**

135 An overview of all instruments used in this campaign to characterize aerosol particles, trace gases, and  
136 meteorological parameters is provided in Table S1. The major instruments used are described in more detail below.

#### 137 **2.2.1 CHARON-PTR-TOF-MS**

138 A proton-transfer-reaction time-of-flight mass spectrometer (PTR-ToF-MS 4000X2, Ionicon Analytik GmbH),  
139 equipped with a particle inlet (Chemical Analysis of aeRosol ONline, CHARON), was utilized to measure VOC  
140 in the gas phase and semi-volatile compounds in the particle phase. The PTR-ToF-MS 4000X2 employed here  
141 has an ion funnel, which reduces ion loss and enhances sensitivity (Pugliese et al., 2020). The CHARON inlet  
142 integrates a gas-phase denuder, an aerodynamic lens with an inertial sampler, and a thermo-desorption unit, all  
143 coupled to a PTR-TOF-MS. The gas-phase denuder removes gas-phase analytes, while the aerodynamic lens  
144 focuses the aerosol particles. The inertial sampler then concentrates the particle-enriched sample flow. Finally,  
145 the particles enter a thermal desorption unit where they are volatilized before being detected by PTR-MS. The  
146 inlet system demonstrated a particle enrichment factor of  $18 \pm 2$  (Figure S3), as discussed in detail in our previous  
147 study (Song et al., 2024). The vaporizer (TDU) was operated at 150 °C and 7-8 mbar absolute pressure. The  
148 CHARON inlet was described in detail elsewhere (Eichler et al., 2015; Muller et al., 2017; Gkatzelis et al., 2018a;  
149 Gkatzelis et al., 2018b).

150 In this campaign, the CHARON-PTR-MS automatically switched between gas and particle phase measurements.  
151 The sequence was: 5 minutes of high-efficiency particulate air (HEPA) filter measurement for particle background,  
152 10 minutes of particle-phase measurement, 3 minutes transition, 10 minutes of gas-phase VOC measurement, and  
153 another 2 minutes transition. The PTR drift tube was kept at 2.7 mbar, 470 V, and 100 °C, with the ion funnel at

154 45 V. These settings correspond to an electric field (E) to gas molecule number density (N) ratio of ~100 Td for  
155 VOC measurement. For particle measurement, the PTR was automatically adjusted to 60 Td.

156 During gas-phase measurement, ambient air was sampled continuously from a 2 m PFA tube (4 mm inner diameter)  
157 at 8 L/min, with 40-100 mL/min directed to the PTR-ToF-MS through a polyetheretherketone (PEEK) tubing at  
158 80°C. The instrumental background was determined weekly at noon by introducing pure dry nitrogen (N<sub>2</sub>,  
159 99.9999%) into the inlet for 5-15 min to exclude ambient air and quantify the instrumental baseline (Figure S4).  
160 For particle-phase measurement, ambient particles were sampled with a PM<sub>2.5</sub> inlet (Comde Dendra) through a  
161 vertical electropolished 3.45 m stainless-steel tube (12 mm inner diameter) at 16.7 L/min, with 550 mL/min  
162 directed to the CHARON inlet. Particle background was automatically determined using the HEPA filter.

163 Gas calibrations were performed at the beginning, middle, and end of each campaign periods using a gas cylinder  
164 (Ionicon Analytik GmbH) with 15 VOC, including toluene, trimethylbenzene, xylene, alpha-pinene, acetone,  
165 acetonitrile, benzene, and isoprene (accuracy 5% at ~1000 ppb). The sensitivity ranged from ~1000 to 4000  
166 cps/ppb for different compounds across different seasonal calibration periods (Figure S5). Raw data from  
167 CHARON-PTR-MS were processed using IONICON Data Analyzer software (IDA 2.2.0) following Müller et al.  
168 (2013), Lannuque et al. (2023), and Peron et al. (2024). The CHARON inlet enrichment factor was determined  
169 via external calibration with size-selected (DMA, TSI) ammonium nitrate particles (100-500 nm) measured by a  
170 condensation particle counter (CPC, TSI).

### 171 **2.2.2 HR-TOF-AMS**

172 A high-resolution time-of-flight Aerosol Mass Spectrometer (HR-ToF-AMS) (Aerodyne Research Inc.),  
173 equipped with a PM<sub>2.5</sub> aerodynamic lens, was used to measure non-refractory PM<sub>2.5</sub> (NR-PM<sub>2.5</sub>) components,  
174 including organic aerosol, nitrate, sulfate, ammonium, and chloride, with a time resolution of 1 minute (Peter F.  
175 Decarlo et al., 2006; Canagaratna et al., 2007; Williams et al., 2013). The operation and calibration procedures of  
176 the AMS are detailed in our previous publications (Huang et al., 2019; Song et al., 2022). The instrument's  
177 capability to provide high-resolution mass spectra enables detailed chemical composition analysis of aerosol  
178 particles in real time. Briefly, ambient air was sampled through a PM<sub>2.5</sub> inlet (flow rate of 1 m<sup>3</sup> h<sup>-1</sup>) that was shared  
179 with the CHARON system via a 3.45 m stainless-steel tube. A subset of this flow was then directed to the HR-  
180 ToF-AMS at a flow rate of 84 cm<sup>3</sup> min<sup>-1</sup>. The aerosol particles were focused into a narrow beam by a PM<sub>2.5</sub>  
181 aerodynamic lens, which effectively transmits particles with vacuum aerodynamic diameters (d<sub>va</sub>) ranging from  
182 ~70 to ~2500 nm. The particles were subsequently heated by a vaporizer at 600 °C, causing the non-refractory  
183 components to volatilize. The volatilized particles were then ionized by electron impact at 70 eV, which is a  
184 standard method for ionizing organic and inorganic compounds, ensuring fragmentation patterns that are well-  
185 characterized and suitable for identification. The AMS was calibrated using dried ammonium nitrate aerosol  
186 particles with sizes of 100-500 nm to determine ionization efficiency and instrument response. Calibration  
187 particles were size-selected using a DMA, and signal stability was verified prior to and during each measurement  
188 period. Data from the AMS were processed and analyzed using the SQUIRREL 1.65G and PIKA 1.25G software  
189 packages. To address the issue of particle bounce losses, a chemical-composition-based collection efficiency (CE)  
190 of approximately 0.5 was applied to calculate the particle mass concentrations (Docherty et al., 2011; Middlebrook  
191 et al., 2012). For the elemental analysis of organic aerosol (OA), including the hydrogen-to-carbon ratio (H: C)

192 and the oxygen-to-carbon ratio (O: C), we utilized the improved ambient method (Allison C. Aiken et al., 2008;  
193 Canagaratna et al., 2015).

### 194 **2.2.3 Other Instruments**

195 The mass concentrations of PM<sub>2.5</sub> and PM<sub>10</sub> and particle size distributions (0.2-18 μm) were determined using an  
196 optical particle counter (Fidas200, Palas). Particle number concentrations (> 2.5 nm) were monitored using a  
197 water-based condensation particle counter (Model 3789, TSI Inc.) and a butanol-based condensation particle  
198 counter CPC3776 (TSI Inc., USA). Particle number size distributions ranging from 10 to 410 nm were measured  
199 using a nanoparticle sizer (Nanoscan 3910; TSI Inc.) at time resolution of 1 min in winter, and distributions  
200 ranging from 13.6 to 763.5 nm were measured using a scanning mobility particle sizer (SMPS; DMA 3081; TSI  
201 Inc.) at a time resolution of 7 min in Summer. Equivalent black carbon (eBC) levels were monitored with an  
202 aethalometer (AE33, Magee Scientific) at a 1-minute resolution. Ammonia (NH<sub>3</sub>) concentrations were measured  
203 via cavity ring-down spectroscopy (G2103, Picarro Inc.). The gas was sampled via a Teflon tube (4 mm i.d.; 3.1s  
204 residence time). Ozone (O<sub>3</sub>) and nitrogen dioxide (NO<sub>2</sub>) concentrations were tracked using the O<sub>3</sub>41M and  
205 AS32M gas analyzers (both from Environment S.A.), respectively. Meteorological parameters such as  
206 temperature, relative humidity, wind speed and direction, global radiation, and precipitation were recorded with a  
207 compact weather sensor (WS700, Lufft) installed on the container roof. Additional meteorological data was  
208 measured by the Institute of Meteorology of the LMU on top of the institute at about 30 m above ground level  
209 (<https://www.meteo.physik.uni-muenchen.de/request-beta/>). The vertical aerosol distribution was assessed using  
210 a scanning aerosol Lidar (Rametris Inc., Type: LR111-ESS-D200, named KASCAL). Fiber laser-induced  
211 fluorescence (FILIF) detects formaldehyde (HCHO) by exciting molecules at 353 nm and measuring fluorescence  
212 above 370 nm. The technique alternates between on-peak and off-peak laser frequencies to determine HCHO  
213 concentration with high specificity. Calibrated against FTIR standards, FILIF achieves ± 27 pptv precision (10-  
214 15% accuracy) at 10 Hz sampling frequency, unaffected by humidity. All the information could be found in  
215 previous studies (Ye et al., 2021). Unless otherwise specified, all measured values are reported as mean ± standard  
216 deviation. Please note that this work is linked to the recently established low-cost sensor network in downtown  
217 Munich, monitoring especially O<sub>3</sub>, NO<sub>2</sub> and PM<sub>2.5</sub> (Chen, 2025). This included frequent comparison  
218 measurements between reference instruments on a bicycle platform, the instruments in our container, a LfU  
219 regulatory monitoring station, and the low-cost sensor network in downtown Munich. Back trajectories were  
220 calculated using the Hybrid Single-Particle Lagrangian Integrated Trajectory (HYSPPLIT) model (Stein et al., 2015)  
221 at 500 m altitude with 72-hour backward duration to identify potential source regions and transport pathways  
222 influencing air quality at the measurement site.

### 223 **2.2.4 PMF analysis**

224 The PMF receptor model is a bilinear algorithm that separates air pollutant time series into sources characterized  
225 by factor profiles, time series, and residuals (Paatero and Tapper, 1994; Paatero, 1999). It is widely used to identify  
226 particle and VOC sources (Kim et al., 2004; Reyes-Villegas et al., 2016; Huang et al., 2018; Gkatzelis et al., 2021).  
227 PMF has also been applied to inorganic aerosol components, elemental composition of particulate matter (PM),  
228 VOC, PAHs, black carbon, and size-resolved particle data, showing its versatility as a receptor model across  
229 various pollutant types (Äijälä et al., 2019). PMF has been used for analyzing high-time-resolution elemental data

230 in PM<sub>2.5</sub> and PM<sub>10</sub> to identify urban and industrial sources and to separate fine and coarse particle sources (Reizer  
231 et al., 2021). Reviews and guidelines from European air quality agencies explicitly mention the use of PMF  
232 applied to particle mass, ions, metals, and gaseous species (like VOC and PAHs) in addition to OA for  
233 comprehensive source apportionment studies (Belis et al., 2013). In summary, PMF receptor modeling is broadly  
234 used and suitable for source apportionment of multi-pollutant data sets.

235 To investigate the sources of VOC, SVOA, and OA, positive matrix factorization (PMF) was applied separately  
236 to (i) VOC mass spectra measured by PTR-MS, (ii) semi-volatile aerosol species measured by CHARON-PTR-  
237 MS, and (iii) OA measured by HR-TOF-AMS. PMF analyses were conducted independently for each dataset and  
238 measurement campaign rather than using a combined dataset. Separate analyses were chosen because the  
239 campaigns were performed in different seasons under substantially different atmospheric conditions and  
240 instrument states. PMF assumes temporally stationary factor profiles and comparable uncertainty structures within  
241 a dataset; these assumptions are not fulfilled when combining measurements across seasons with distinct source  
242 contributions and atmospheric processing regimes. In addition, VOC and SVOA datasets were analyzed separately  
243 because they represent chemically and physically distinct phases with different atmospheric processing timescales,  
244 variability patterns, and measurement uncertainty structures. Combining these datasets in a single PMF analysis  
245 would violate the assumption of consistent covariance structure and could lead to mixed or non-interpretable  
246 factors. Diagnostic evaluations supporting solution stability and factor selection for each dataset are provided in  
247 the Supplement (Figures S8-S20). For VOC-PMF, inputs were derived from PTR-TOF-MS data following the  
248 methodology of Song et al. (2024), involving comprehensive preprocessing including mass spectral deconvolution,  
249 background subtraction, and error matrix calculation where uncertainties were determined as  
250  $[(0.1 \times \text{concentration})^2 + (0.5 \times \text{LOD})^2]^{1/2}$  (Kajos et al., 2015). SVOA-PMF inputs were obtained through two  
251 complementary measurement modes: HEPA-filtered air samples (representing background signals) and direct  
252 atmospheric sampling (Dir) capturing real-time conditions, with ions (primarily C<sub>x</sub>H<sub>y</sub><sup>+</sup>, C<sub>x</sub>H<sub>y</sub>O<sub>z</sub><sup>+</sup>, and C<sub>x</sub>H<sub>y</sub>O<sub>z</sub>N<sub>n</sub><sup>+</sup>).  
253 Both datasets underwent rigorous quality control procedures. Low-molecular-weight species ( $m/z \leq 60$ ) were  
254 excluded to eliminate potential interferences from fragments and common atmospheric gases that may not be  
255 representative of specific emission sources (Zhang et al., 2011). Additionally, compounds with  $\geq 20\%$  missing  
256 data points were removed to ensure statistical robustness in the PMF analysis, following established protocols for  
257 PMF data preparation (Ulbrich et al., 2009; Zhang et al., 2011). The analyses were initially processed using SoFi  
258 Pro 9.0 (Datalystica Ltd.) for exploratory factor analysis and data visualization. The source apportionment of  
259 organic aerosols ( $m/z$  12-120) was then conducted through unconstrained AMS-PMF analysis using the PMF  
260 Evaluation Tool (v3.08C) within IGOR Pro (v8.04), which maintains legacy algorithms specifically optimized for  
261 AMS datasets, particularly for handling nonlinear  $m/z$  signal-uncertainty relationships in typical AMS operating  
262 conditions.

263 The final number of factors for each dataset was selected based on a combination of diagnostic criteria, including  
264 the evolution of  $Q/Q_{\text{exp}}$  values, inspection of scaled residual distributions, physical interpretability of factor  
265 profiles, and temporal behavior. Physical interpretability was evaluated using dominant marker compounds in  
266 each factor mass spectrum together with their temporal patterns, allowing source attribution based on established  
267 source signatures (e.g., traffic-related factors identified by toluene/xylene dominance and rush-hour diurnal peaks).  
268 Solutions with increasing factor numbers were examined to identify the point beyond which additional factors

269 primarily resulted in factor splitting without meaningful improvement in residual structure. Detailed diagnostics,  
270 including  $Q/Q_{\text{exp}}$  evolution, residual analysis,  $F_{\text{peak}}$  sensitivity tests, and correlations with characteristic  
271 compound markers and diurnal patterns, are provided in the Supplement (Section S3.2, Figures S7 – S19, Table  
272 S4 – S9).

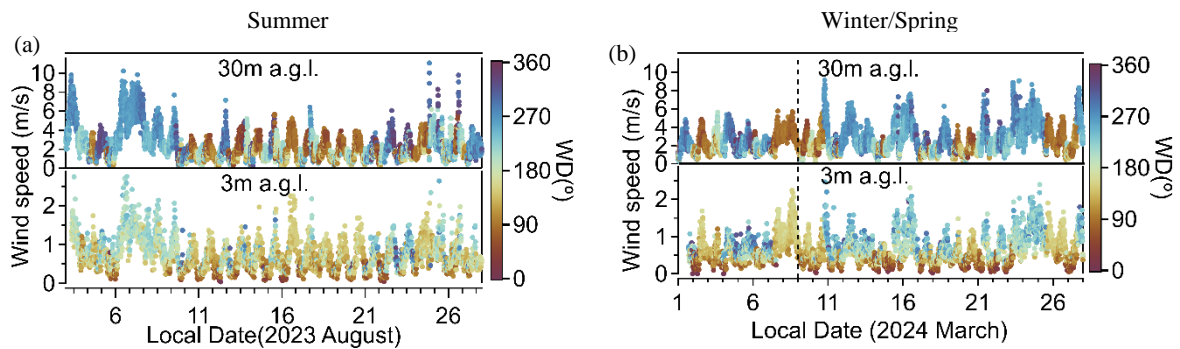
### 273 3. Results and discussion

274 In the first section, we give an overview of the meteorological conditions during the two measurement campaigns  
275 and the main characteristics of the observed evolution of aerosol particles and trace gases. The second section will  
276 discuss the major sources of aerosol particles and trace gases. In the third section, we focus on strong biomass  
277 burning events.

#### 278 3.1 Overview of observations during summer and wintertime

##### 279 3.1.1 Overview of meteorological and particle observations

280 The summer period was characterized by frequent sunny weather with moderate to high temperatures and  
281 significant precipitation events mainly at the beginning and end of the summer campaign. The late winter/spring  
282 period shows typical winter conditions until March 8<sup>th</sup>, according to temperature, precipitation followed by more  
283 spring-like conditions thereafter.



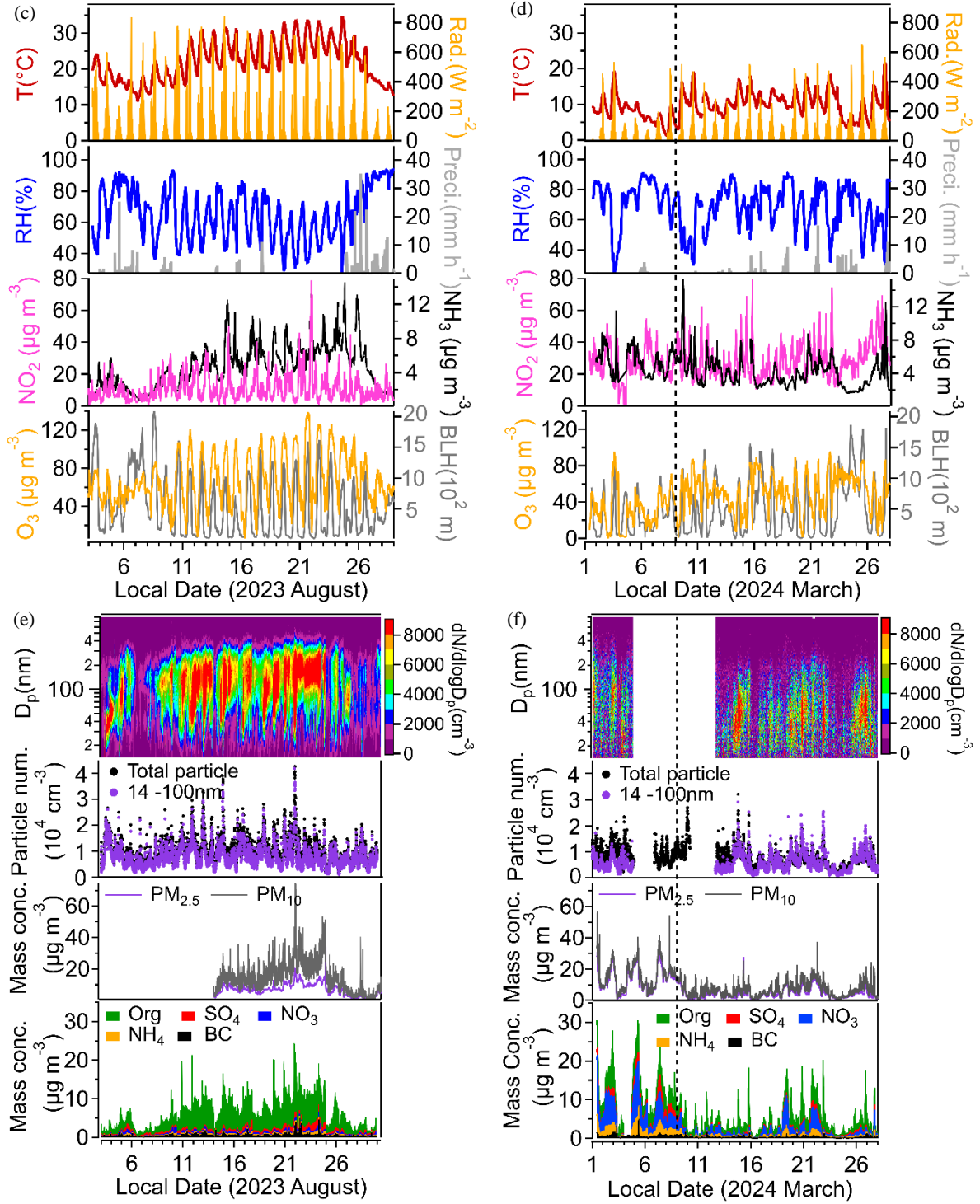


**Figure 1:** Time series of wind speed & direction 3m (above ground level) and 30 m (above ground level) in summer (a) and winter (b); temperature (T); global radiation (Ra); relative humidity (RH); precipitation;  $NO_2$ ;  $NH_3$ ;  $O_3$  and boundary layer height (BLH\*) in summer (c) and winter (d); Particle number size distributions; particle number of total and below 100nm ultrafine particles;  $PM_{2.5}$  and  $PM_{10}$  mass concentrations; Organic aerosol (OA), sulfate, nitrate, and ammonium; Equivalent black Carbon (eBC) in summer (e) and (f) in winter; #All data plotted except the wind data were measured at the container roof. \*Please note that the BLH data refer to ERA5 reanalysis data (Guo et al., 2024), which represent large-scale boundary layer conditions and may not fully capture street-canyon ventilation or local turbulence effects. The vertical dotted line marks the transition between the late-winter and early-spring periods, defined based on observed changes in temperature, solar radiation, and aerosol chemical composition.

284 Wind measurements at 3 m and 30 m above ground (Figure 1a-b) revealed consistent vertical gradients across all  
285 seasons, with average speeds of  $0.7 \pm 0.4$  and  $2.6 \pm 1.4$  m s<sup>-1</sup>, respectively. Meteorological conditions varied  
286 significantly between seasons (Figure 1c-d), creating distinct chemical environments. The higher summer  
287 temperatures ( $21.9 \pm 5.8$  °C) promoted enhanced biogenic emissions and photochemical activity, while lower  
288 winter temperatures ( $8.4 \pm 3.0$  °C) favored primary pollutant accumulation. Relative humidity and total  
289 precipitation showed minimal seasonal variation. NO<sub>2</sub> concentrations were 2.5-2.8 times higher in winter/spring  
290 ( $26.1 \pm 9.9$  /  $28.4 \pm 10.8$  µg m<sup>-3</sup>) than summer ( $10.2 \pm 7.7$  µg m<sup>-3</sup>) due to increased heating emissions and reduced  
291 photolysis under shallow boundary layers ( $339 \pm 298$  m /  $510 \pm 477$  m vs  $516 \pm 453$  m, variability). The BLH  
292 values are derived from ERA5 reanalysis and represent regional-scale atmospheric mixing. They do not resolve  
293 street-canyon ventilation. In a street canyon, buildings can limit horizontal and vertical dispersion, especially  
294 under stable winter conditions. Therefore, pollutant accumulation at the measurement site may be stronger than  
295 suggested by ERA5 BLH alone. This limitation is particularly relevant for reactive pollutants such as NO<sub>2</sub>. In  
296 addition to dispersion, NO<sub>2</sub> is strongly influenced by local traffic emissions and rapid photochemical processes  
297 (e.g., photolysis and O<sub>3</sub> titration). As a result, short-term variations in NO<sub>2</sub> may reflect a combination of street-  
298 canyon trapping, advection, and chemical transformation. This can differ from more inert traffic-related species  
299 such as BC, which are primarily governed by physical mixing. The ERA5 BLH should therefore be interpreted as  
300 an indicator of large-scale mixing conditions rather than street-level ventilation. The LfU station showed similar  
301 winter ( $27.2 \pm 9.2$  µg m<sup>-3</sup>) and early spring ( $27.8 \pm 9.2$  µg m<sup>-3</sup>) mean concentrations to Theresienstrasse, but  
302 exhibited weak temporal correlation, reflecting the strong spatial variability of NO<sub>2</sub>. Notably, summer NO<sub>2</sub> at LfU  
303 ( $23.4 \pm 10.1$  µg m<sup>-3</sup>) was 2.3 times higher than Theresienstrasse, yet temporal correlation improved substantially  
304 ( $R = 0.5$ ) in Figure S6. This seasonal pattern suggests that summer's higher boundary layer enhanced vertical  
305 mixing and local photochemical reactions, increasing spatial differences in mean NO<sub>2</sub> levels. However, stronger  
306 synchronized daily photochemical cycles improved temporal agreement between the two sites. The diurnal  
307 evolution of NO<sub>2</sub>, O<sub>3</sub>, and BLH reveals seasonally distinct coupling between photochemical processing and  
308 boundary-layer mixing (Figure S7). During summer, increasing BLH coincides with decreasing NO<sub>2</sub>  
309 concentrations and enhanced daytime O<sub>3</sub> formation, indicating efficient vertical mixing and active photochemical  
310 processing. Spring exhibits intermediate behavior, whereas winter shows weaker BLH development and  
311 persistently elevated NO<sub>2</sub> levels consistent with reduced photolysis and limited dispersion. Gaseous NH<sub>3</sub> showed  
312 elevated concentrations across all seasons, with winter ( $5.4 \pm 1.5$  µg m<sup>-3</sup>) and spring ( $4.0 \pm 1.8$  µg m<sup>-3</sup>) levels  
313 comparable to summer values ( $4.8 \pm 2.6$  µg m<sup>-3</sup>). O<sub>3</sub> concentrations at Theresienstrasse exhibited strong seasonal  
314 variation, with highest levels in summer ( $67.1 \pm 26.6$  µg m<sup>-3</sup>), followed by early spring ( $52.2 \pm 19.3$  µg m<sup>-3</sup>), and  
315 lowest in late winter ( $32.4 \pm 20.2$  µg m<sup>-3</sup>). The LfU station showed similar seasonal patterns (summer:  $59.3 \pm 25.5$   
316 µg m<sup>-3</sup>; late winter:  $30.8 \pm 17.3$  µg m<sup>-3</sup>; early spring:  $45.9 \pm 17.2$  µg m<sup>-3</sup>) with strong temporal correlations ( $R =$   
317  $0.8$  in August 2023;  $R = 0.7$  in March 2024) in Figure S6, indicating consistent O<sub>3</sub> behavior across both sites  
318 driven by regional photochemical processes.

319 Particle size distributions revealed contrasting seasonal patterns driven by different formation mechanisms  
320 (Figures 1e-f). Summer showed the highest total particle number concentrations ( $10000 \pm 5100$  cm<sup>-3</sup>) with a  
321 substantial variability dominated by ultrafine particles (< 100 nm:  $80.6 \pm 8.2\%$ ), indicating a strong contribution  
322 of ultrafine particles during this period. Winter exhibited lower total number concentrations ( $8900 \pm 3500$  cm<sup>-3</sup>)

323 and a lower fraction of ultrafine particles ( $33.6 \pm 10.1\%$ ), consistent with a greater relative contribution of aged  
 324 and accumulation-mode particles under stable conditions. Spring showed intermediate behavior with high  
 325 ultrafine fractions (89.7%) but lower absolute number concentrations. The seasonal PM mass concentrations  
 326 showed opposite trends to the particle number concentrations: winter PM<sub>2.5</sub> peaked at  $13.0 \pm 7.4 \mu\text{g m}^{-3}$  with  
 327 nitrate as the dominant component due to low temperatures, shallow boundary layers and increased residential  
 328 heating. In contrast, summer ( $6.7 \pm 3.7 \mu\text{g m}^{-3}$ ) and spring ( $4.2 \pm 3.1 \mu\text{g m}^{-3}$ ) showed lower PM<sub>2.5</sub> levels dominated  
 329 by organic aerosols, despite higher particle numbers, highlighting that ultrafine particles can dominate number  
 330 concentrations in urban environments while contributing comparatively little to total particulate mass.

331 Aerosol particle mass composition varies significantly by season, reflecting different formation mechanisms.  
 332 Organic aerosol particles dominate in summer due to high photochemical activity (Figures 2), averaging  $4.3 \pm 2.9$   
 333  $\mu\text{g m}^{-3}$ , higher than  $3.3 \pm 1.7 \mu\text{g m}^{-3}$  in winter and  $1.8 \pm 1.8 \mu\text{g m}^{-3}$  in spring. Nitrate is the main component in  
 334 winter ( $4.5 \pm 3.2 \mu\text{g m}^{-3}$ ) due to low temperatures favoring particle phase and increased heating emissions  
 335 providing abundant NH<sub>3</sub> and NO<sub>x</sub> precursors for ammonium nitrate formation. Nitrate concentrations drop  
 336 significantly in spring ( $1.0 \pm 1.3 \mu\text{g m}^{-3}$ ) and summer ( $0.3 \pm 0.2 \mu\text{g m}^{-3}$ ) as rising temperatures shift the equilibrium  
 337 toward the gas phase. Ammonium follows similar patterns, peaking in winter ( $1.8 \pm 1.1 \mu\text{g m}^{-3}$ ) and remaining  
 338 low in warmer seasons (spring:  $0.4 \pm 0.4 \mu\text{g m}^{-3}$ ; summer:  $0.3 \pm 0.2 \mu\text{g m}^{-3}$ ), consistent with reduced ammonium  
 339 nitrate formation.

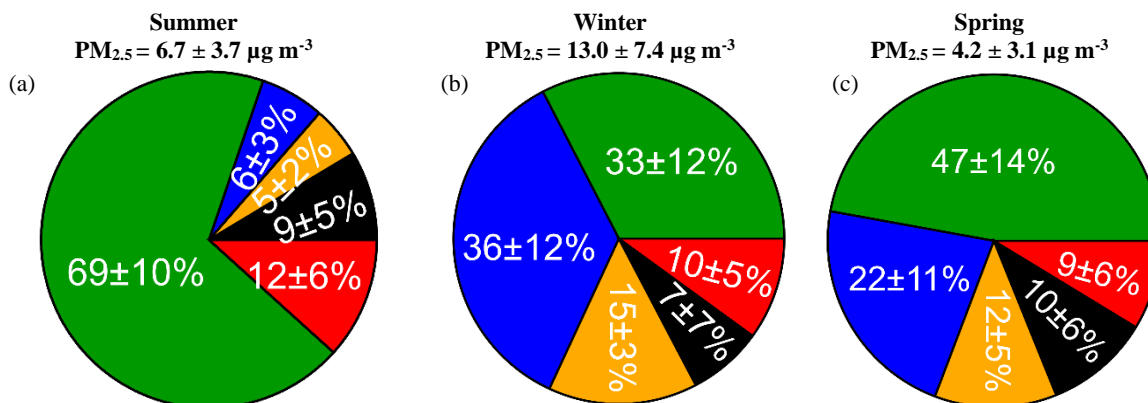


**Figure 2:** Average fractions of PM<sub>2.5</sub>: OA (green), sulfate (red), nitrate (blue), ammonium (yellow) and eBC (black) in summer (a), (b) in winter (until March 8<sup>th</sup>) and (c) in spring based on AMS and Aethalometer measurements.

### 340 3.1.2 Diurnal behaviour of gaseous BVOC and BTEX

341 The average diurnal variations of key volatile organic compounds (VOC) are examined below, focusing on major  
 342 biogenic and anthropogenic species, including BTEX—a group of aromatic hydrocarbons comprising benzene,  
 343 toluene, ethylbenzene, and xylene. The VOC selected here comprise  $32.3 \pm 13.1\%$  of all VOC detected in summer,  
 344  $41.0 \pm 12.9\%$  in winter and  $37.9 \pm 12.5\%$  in spring.

345 Figure 3 illustrates the diurnal variations of six VOC across three seasons, revealing distinct patterns tied to their  
 346 sources and environmental influences. Isoprene and monoterpenes, both biogenic VOC, exhibit the highest mixing  
 347 ratios in summer. However, Isoprene displays a bimodal pattern in summer and spring, with concentration peaks  
 348 during the morning and evening hours, suggesting a potential link to traffic activity during the morning and  
 349 evening hours. This is consistent with direct measurements of isoprene in vehicle exhaust by Borbon et al. (2001).  
 350 Additionally, fragmentation of higher-carbon aldehydes and cycloalkanes from anthropogenic sources may

351 contribute to the signal of isoprene, further complicating source attribution in urban environments (Coggon et al.,  
 352 2024b). Monoterpene exhibited early morning peaks in summer and spring, but was almost flat in winter. In  
 353 contrast, their concentrations are minimal in winter due to suppressed biological activity. Anthropogenic VOC  
 354 like benzene, toluene, xylene, and trimethylbenzene show different seasonal behaviors. Benzene peaks in winter,  
 355 likely due to lower BLH and reduced dispersion, with dips at midday possibly from increased OH radical oxidation  
 356 under sunlight. Toluene, xylene, and trimethylbenzene display notable spikes in spring, particularly during  
 357 morning and evening hours, suggesting strong contributions from traffic emissions and industrial activities.

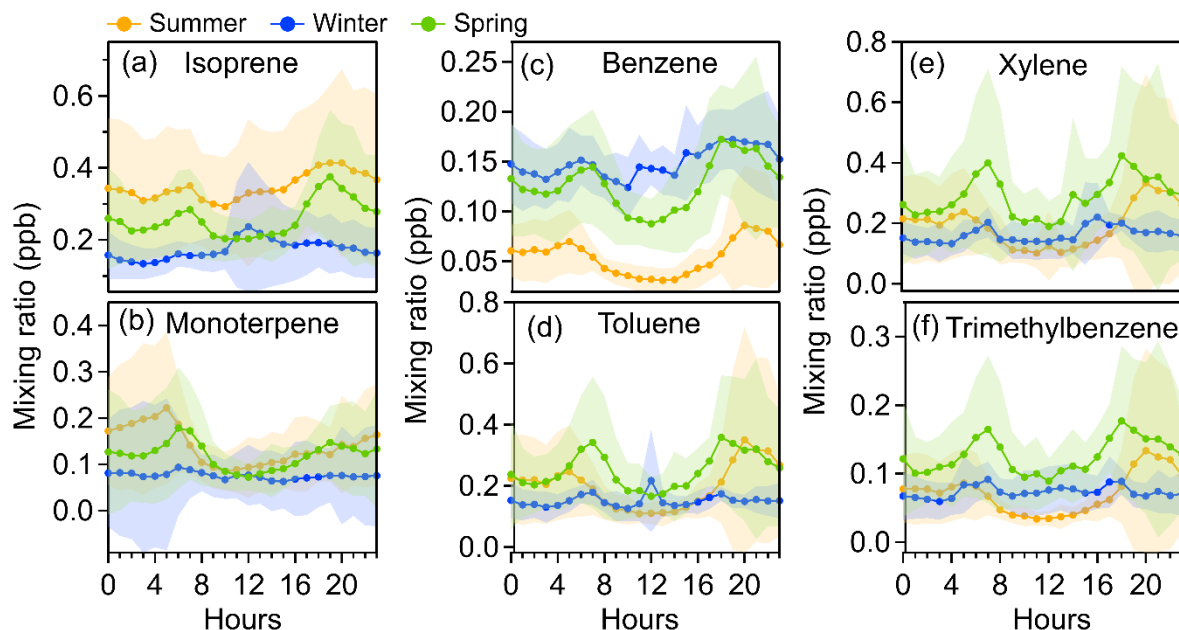


Figure 3: Diurnal behavior of (a) Isoprene, (b) Monoterpenes, (c) Benzene, (d) Toluene, (e) Xylene and (f) Trimethylbenzene in summer, winter and spring.

### 358 3.2 Sources of VOC and organic aerosol particles

359 In this section we use statistical (PMF) analysis of on-line mass spectra from VOC (PTR-MS) and semi-volatile  
 360 organic aerosol particles (CHARON-PTR-MS) as well as organic aerosol particles (HR-TOF-AMS) to determine  
 361 their major sources.

#### 362 3.2.1 VOC sources in summer and winter

363 We included 117 VOC ions (Table S2) for PMF analysis in summer and 97 VOC ions (Table S3) in winter/spring.  
 364 Ions with extremely high signal intensities that could disproportionately influence the PMF solution, as well as  
 365 very low signal ions with minimal contribution, were excluded. The excluded high-abundance ions are common  
 366 hydrocarbon and oxygenated VOC fragments, such as  $m/z$  33.034 ( $C_1H_5O^+$ ), 41.039 ( $C_3H_5^+$ ), 43.054 ( $C_3H_7^+$ ),  
 367 45.034 ( $C_2H_5O^+$ ), 57.070 ( $C_4H_9^+$ ), and 59.049 ( $C_3H_7O^+$ ). These ions were removed because their high  
 368 concentrations may lead to over-representation of specific factors, whereas low-signal ions were excluded to  
 369 reduce noise interference (Song et al., 2024). The average VOC molecules mixing ratio is  $3.4 \pm 1.0$  ppb in summer,  
 370  $2.1 \pm 0.7$  ppb in winter, and  $3.4 \pm 1.7$  ppb in spring. This study thoroughly examined factor profiles, diurnal  
 371 patterns, and correlations with tracers (Figure 4, S8 and Table S4) for summer and for winter (Figures S9, S10  
 372 and Table S5). Five factors were identified based on measured VOC as the optimal interpretable solutions for  
 373 summer and winter, respectively.

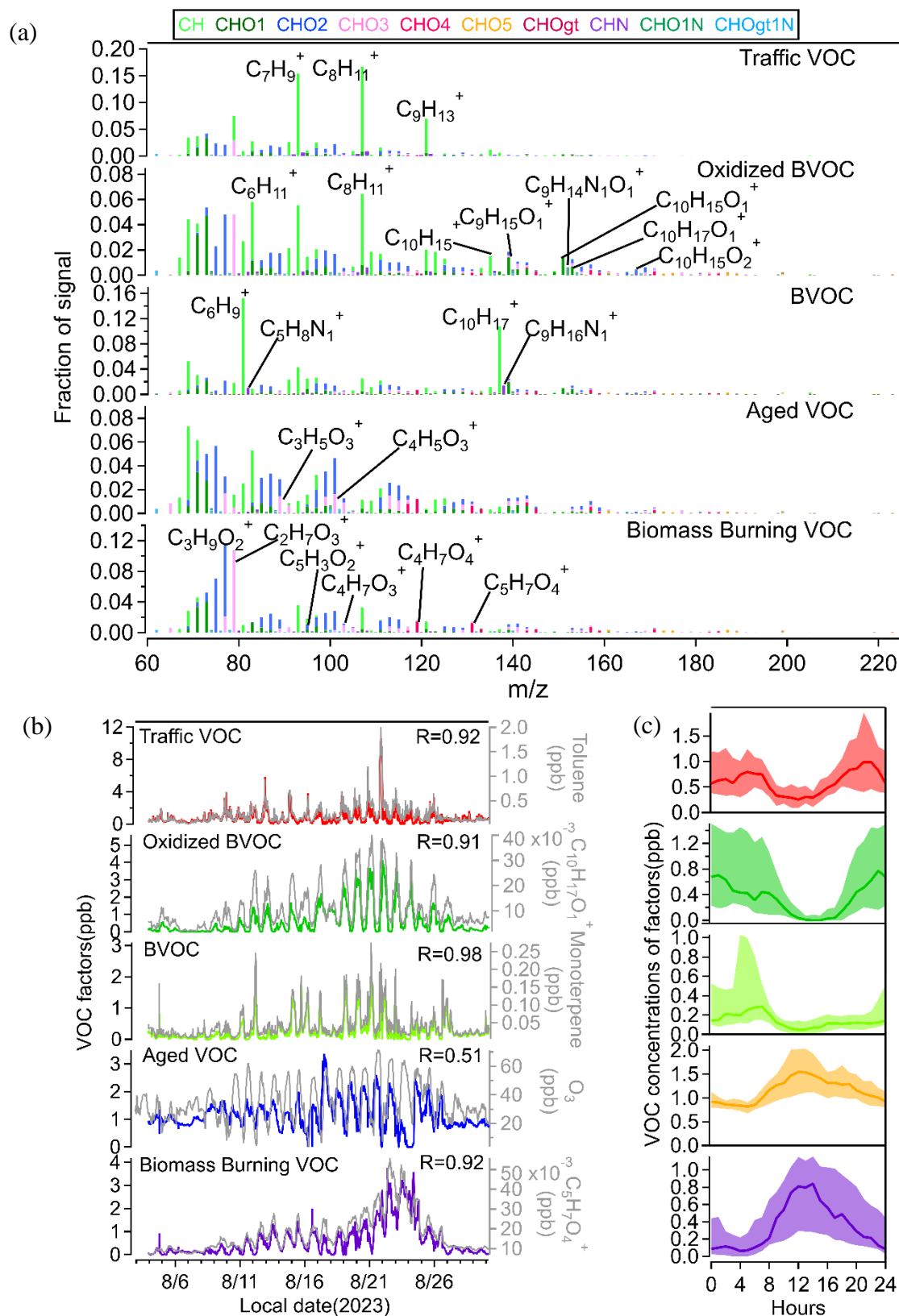


**Figure 4** VOC source apportionment for summer time. (a) Normalized VOC factor mass spectra from PMF analysis and characteristic mass peaks in summer; (b) Time series of VOC factors including traffic, oxidized BVOC, BVOC, aged VOC, and biomass burning VOC; (c) Median diurnal variations in VOC factors during summer time

374 In summer, the first factor was characterized by high contributions and strong correlations with aromatic  
 375 hydrocarbon ions, such as  $C_7H_9^+$  ( $m/z$  93.07),  $C_8H_{11}^+$  ( $m/z$  107.086), and  $C_9H_{13}^+$  ( $m/z$  121.102). These compounds

376 correspond to toluene, xylenes, and C<sub>9</sub>-aromatics, commonly used as vehicular emission markers (Squires et al.,  
377 2020; Jain et al., 2022). We assigned it to traffic VOC. These ions show a correlation coefficient (R) of  
378 approximately 0.9 with traffic emissions (Table S3). According to the diurnal profiles of traffic (Figure 4) in  
379 summer, it shows distinct peaks during morning and evening hours.

380 The second factor was classified as weakly oxidized BVOC. It was identified by oxidation products of  
381 monoterpenes, specifically C<sub>9</sub>H<sub>15</sub>O<sub>1</sub><sup>+</sup> myrcenol (m/z 139.112), C<sub>10</sub>H<sub>13</sub>O<sub>1</sub><sup>+</sup> carvone (m/z 149.097), weakly-oxidized  
382 molecules of monoterpenes C<sub>10</sub>H<sub>15</sub>O<sub>1</sub><sup>+</sup> (m/z 151.112), C<sub>10</sub>H<sub>17</sub>O<sub>1</sub><sup>+</sup> (m/z 153.128) and C<sub>10</sub>H<sub>15</sub>O<sub>2</sub><sup>+</sup> (m/z 167.107) (Li  
383 et al., 2020a). These ions show strong correlations with the Oxidized BVOC factor, with R values of 0.93, 0.93,  
384 0.93, 0.91, and 0.87, respectively. Oxidized BVOC have a nighttime peak in the diurnal profile and drop to nearly  
385 zero by noon, likely due to enhanced dilution and quicker oxidation to oxidation states not detectable by PTR-  
386 MS.

387 The third factor was identified as BVOC due to the predominance of C<sub>10</sub>H<sub>17</sub><sup>+</sup> monoterpene (m/z 137.133) and its  
388 fragmentation C<sub>6</sub>H<sub>9</sub><sup>+</sup> (m/z 81.07) ions in this VOC factor, with correlations of 0.98 and 0.86, respectively.  
389 Sesquiterpenes also show a strong correlation with this factor (R=0.80). The average diurnal behavior of BVOC  
390 shows an early morning peak, because BVOC, especially monoterpenes, are often stored in vegetation and  
391 released at the start of the morning due to sunlight and slight temperature increases (Malik et al., 2023), combined  
392 with a shallow boundary layer that keeps emissions near the surface.

393 The fourth factor showed a good correlation with butyric acid C<sub>3</sub>H<sub>5</sub>O<sub>3</sub><sup>+</sup> (m/z 89.024) and C<sub>4</sub>H<sub>5</sub>O<sub>3</sub><sup>+</sup> (m/z 101.024),  
394 with R values of 0.75 and 0.72, respectively. The time series of O<sub>3</sub> and this factor showed a good correlation  
395 during certain periods. The diurnal cycle of it exhibits a daytime peak, indicating involvement in photochemical  
396 oxidation processes. We classified it as aged VOC.

397 The fifth factor, biomass burning VOC, is dominated by propylene glycol C<sub>3</sub>H<sub>9</sub>O<sub>2</sub><sup>+</sup> (m/z 77.06) and orthoacetic  
398 acid C<sub>2</sub>H<sub>7</sub>O<sub>3</sub><sup>+</sup> (m/z 79.039), with strong correlations of 0.85 and 0.83, respectively. Additionally, a ring fragment  
399 of oxidized syringol, C<sub>4</sub>H<sub>7</sub>O<sub>4</sub><sup>+</sup> (m/z 119.034), and ring fragments of oxidized guaiacol and syringol molecules  
400 C<sub>5</sub>H<sub>3</sub>O<sub>2</sub><sup>+</sup> (m/z 95.013), C<sub>5</sub>H<sub>7</sub>O<sub>4</sub><sup>+</sup> (m/z 131.034) and C<sub>4</sub>H<sub>7</sub>O<sub>3</sub><sup>+</sup> (m/z 103.04) contribute smaller fractions but display  
401 even higher correlations, with values of 0.90, 0.91, 0.92 and 0.86 (Yee et al., 2013). Compared with the other 4  
402 factors, the biomass burning VOC mass spectrum has more oxidized compounds.

403 In late winter and early spring, the first factor was identified as traffic VOC using the same method as in summer,  
404 showing high contributions and strong correlations with aromatic hydrocarbon ions, including toluene C<sub>7</sub>H<sub>9</sub><sup>+</sup> (m/z  
405 93.07), C<sub>9</sub> aromatics C<sub>9</sub>H<sub>13</sub><sup>+</sup> (m/z 121.102), and cymene C<sub>10</sub>H<sub>13</sub><sup>+</sup> (m/z 133.102) in Figures S7, S8 and Table S5.

406 The second factor, classified as terpenes VOC, was marked by the predominance of monoterpene C<sub>10</sub>H<sub>17</sub><sup>+</sup> (m/z  
407 137.133) and its fragment C<sub>6</sub>H<sub>9</sub><sup>+</sup> (m/z 81.07) ions with correlations of 0.90 and 0.89, respectively. Sesquiterpenes  
408 also show a strong correlation (R=0.92). The diurnal variation shows both morning and evening peaks, with the  
409 morning peak being higher than the evening peak. This pattern differs from typical traffic trends. This pattern is  
410 similar to that of limonene from shower gels (Yeoman et al., 2020), which shows higher concentrations in the  
411 morning compared to the evening. It correlates with the traffic factor because people typically shower in the  
412 morning before leaving home, leading to higher detection. By the evening, the limonene has dissipated.

413 The biomass burning VOC factor included a lot of smaller oxygenated VOC (OVOC) such as 1,3-propanediol  
414 C<sub>3</sub>H<sub>9</sub>O<sub>2</sub><sup>+</sup> (m/z 77.06), acetic anhydride C<sub>4</sub>H<sub>7</sub>O<sub>3</sub><sup>+</sup> (m/z 103.04), 2-furoic acid C<sub>5</sub>H<sub>5</sub>O<sub>3</sub><sup>+</sup> (m/z 113.024), maleic acid  
415 C<sub>4</sub>H<sub>5</sub>O<sub>4</sub><sup>+</sup> (m/z 117.019), butanedioic acid C<sub>4</sub>H<sub>7</sub>O<sub>4</sub><sup>+</sup> (m/z 119.034), benzoic acid C<sub>7</sub>H<sub>7</sub>O<sub>2</sub><sup>+</sup> (m/z 123.045) (Lemieux

416 et al., 2004) and salicylic acid  $C_7H_7O_3^+$  (m/z 139.04). They all show strong correlations ( $R=0.85-0.90$ ) with this  
417 factor. Notably,  $C_5H_5O_3^+$  and  $C_7H_7O_3^+$  are recognized as tracers of biomass burning VOC (Li et al., 2020b;  
418 Romanias et al., 2024). It displays a peak during the daytime, possibly due to biomass burning activities in certain  
419 areas (e.g., cooking or outdoor grilling), which increase VOC emissions and lead to a daytime peak in the VOC  
420 diurnal profile.

421 The fourth factor was dominated by xylene, represented by  $C_8$ -aromatic hydrocarbon  $C_8H_{11}^+$  (m/z 107.086), with  
422 a correlation of 0.96. This factor also shows a strong correlation with 3-ethyl-pyridine  $C_7H_{10}N_1^+$  (m/z 108.081)  
423 and the  $C_9$ -aromatic hydrocarbon VOC  $C_9H_{13}^+$  (m/z 121.102), with correlations of 0.98 and 0.91, respectively.  
424 Xylene and trimethylbenzene are components of flue gases from fossil fuel combustion VOC (Niu et al., 2021).  
425 It also displays morning and evening peaks in its diurnal cycle, leading to its identification as a traffic2 VOC.

426 The fifth factor has minimal correlation with most masses, only showing a correlation of 0.73 with benzene ( $C_6H_7^+$ )  
427 and weak correlations with various oxygenated compounds. Therefore, this factor may originate from different  
428 low-concentration emission sources. Its diurnal variation shows a small evening peak, likely influenced by traffic  
429 or industrial emissions. This factor accounts for  $54\% \pm 9\%$  in late winter, decreasing to  $23\% \pm 16\%$  in early spring  
430 due to the increased temperature (Figure 5), and as background VOC are commonly found to have a high  
431 proportion, we classify it as background VOC.

432 The source contributions of VOC vary significantly across seasons, reflecting shifts in emission patterns and  
433 atmospheric conditions. In summer, the largest contributor is aged VOC at  $42 \pm 18\%$ , indicating the dominance  
434 of secondary pollutants formed through atmospheric photochemical oxidation processing. Traffic emissions  
435 account for  $22 \pm 14\%$ , while oxidized biogenic VOC make up  $13 \pm 13\%$ , and fresh BVOC contribute  $7 \pm 7\%$ .  
436 Biomass burning plays a notable role at  $16 \pm 15\%$ , likely due to outdoor barbeque in warmer months. Winter  
437 exhibits a different profile, with background sources dominating at  $54 \pm 9\%$ , suggesting stable atmospheric  
438 conditions. Traffic-related emissions split into two categories—traffic1 ( $26 \pm 6\%$ ) and traffic2 ( $7 \pm 6\%$ )—possibly  
439 reflecting different vehicle types or fuel usage patterns. Monoterpenes VOC remain low ( $4 \pm 4\%$ ), consistent with  
440 reduced biogenic activity and from anthropogenic source like personal care products (Wu et al., 2024), while  
441 biomass burning contributes  $8 \pm 6\%$ , potentially from residential heating. In spring, the contributions are traffic1  
442  $22 \pm 7\%$ , monoterpene VOC increased to  $9 \pm 9\%$  as vegetation becomes more active, biomass burning VOC  $33 \pm$   
443  $14\%$ , traffic2  $13 \pm 8\%$ , and background  $23 \pm 16\%$  (Figure 5).

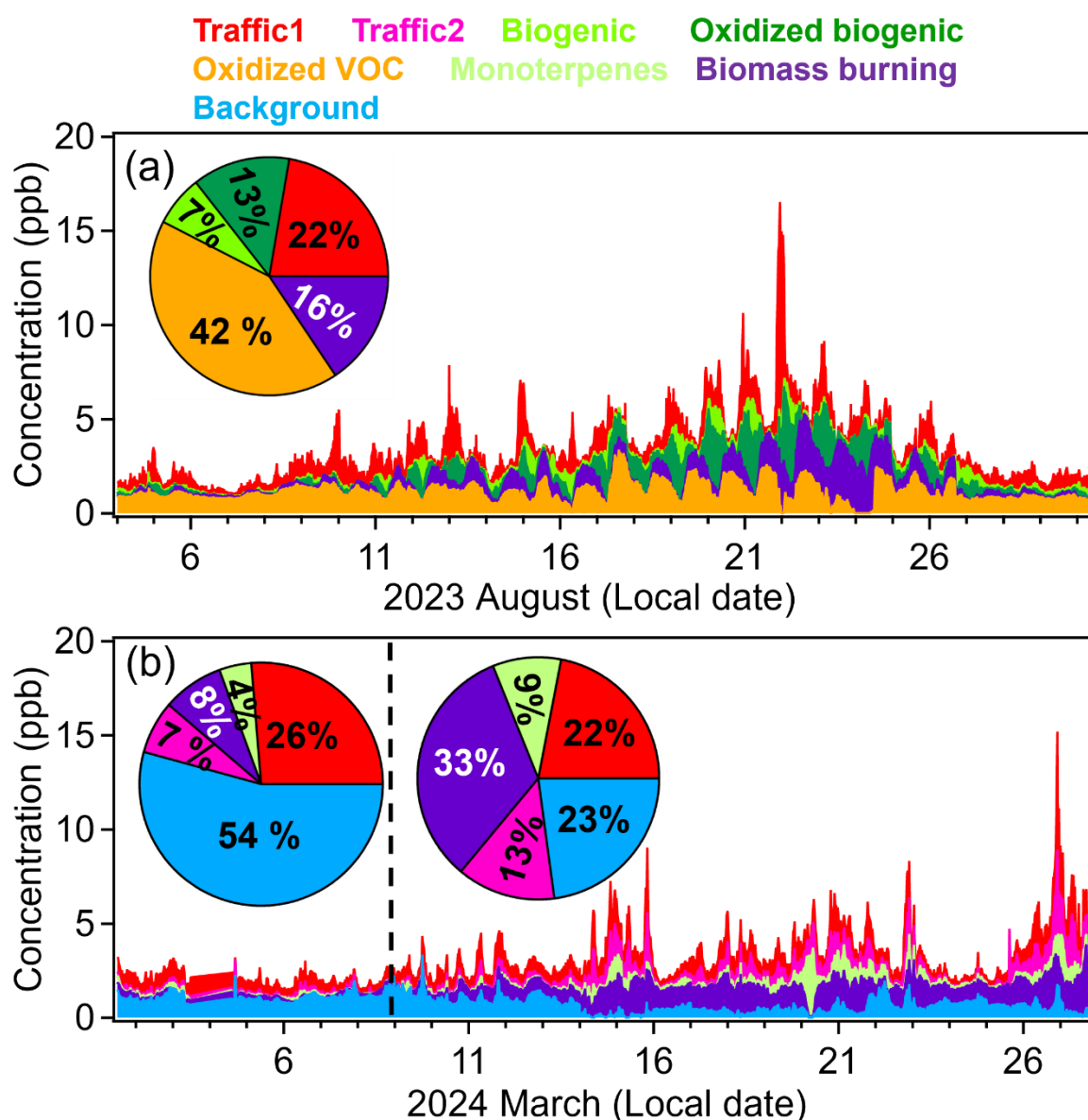


**Figure 5: The time series and relative mass contribution (pie charts) of each VOC factor to total VOC concentrations in summer (a), winter (left of the dash line) and spring (right of the dash line) (b).**

### 444 3.2.2 Sources of semi-volatile organic aerosol (SVOA)

445 We included 153 SVOA ions (Table S6) for PMF analysis for summer and 171 SVOA ions (Table S7) for  
 446 winter/spring, excluding abundant ions that could skew results and very low ion signals with minimal impact  
 447 (Song et al., 2024). The average semi-volatile organic aerosol concentration was  $0.3 \pm 0.2 \mu\text{g m}^{-3}$  in summer,  $0.14$   
 448  $\pm 0.08 \mu\text{g m}^{-3}$  in winter and  $0.07 \pm 0.07 \mu\text{g m}^{-3}$  in spring. Through a comprehensive analysis of factor profiles,  
 449 diurnal variations, and tracer correlations in summer (Figure S11, S12, and Table S8) and in winter (Figure S13,  
 450 S14, and Table S9). Five semi-volatile organic aerosol (SVOA) factors were identified as the best interpretable  
 451 solution for different seasons.

452 In summer, the first factor showed distinct signals from primary oxidation products of terpenes, including oxidized  
 453 monoterpenes  $\text{C}_{10}\text{H}_{15}\text{O}_1^+$  ( $R=0.93$ ) and  $\text{C}_{10}\text{H}_{17}\text{O}_1^+$  ( $R=0.89$ ) (Li et al., 2020a). While the expected monoterpene  
 454 oxidation products are typically  $\text{C}_9\text{H}_{15}\text{O}_{1.5}^+$ , we found that  $\text{C}_9\text{H}_{13}\text{O}_1^+$  and  $\text{C}_9\text{H}_{13}\text{O}_2^+$  also correlated well with this

455 factor, with correlation coefficients  $R=0.91$  and  $R=0.85$ , respectively. This suggests that the  $C_9H_{15}O_{1-2}^+$   
456 compounds may lose hydrogen, forming  $C_9H_{13}O_1^+$  and  $C_9H_{13}O_2^+$  (Gkatzelis et al., 2018b). Additionally, nitrogen-  
457 containing species like  $C_9H_{13}N_1O_1$ ,  $C_9H_{12}N_1O_2$ , and  $C_9H_{13}N_1O_5$  displayed high intensity and significant  
458 correlation with this factor, which may indicate they are fragments of monoterpene-derived organic nitrates, such  
459 as  $C_9H_{15}N_1O_{5.7}$  (Massoli et al., 2018). The diurnal cycle shows a nighttime peak (Figure S10c), which we have  
460 attributed this factor to weakly oxidized biogenic organic aerosol (Weakly OBOA) based on the presence of a  
461 monoterpene oxidation tracer and the observed diurnal pattern.

462 The second factor includes clear markers of isoprene oxidation products, specifically  $C_5H_8O_n$  species (Li et al.,  
463 2020a), with  $C_5H_9O_6^+$  ( $R=0.83$ ) and  $C_5H_9O_3^+$  ( $R=0.82$ ) showing strong correlations (Riva et al., 2016).  
464 Additionally, the ion with the highest fraction,  $C_3H_5O_4^+$  ( $R=0.85$ ), likely originates from the oxidation of  
465 ISOPOOH (Rios, 2018). However, benzoic acid  $C_7H_7O_2^+$  ( $R=0.95$ ), showing a strong signal, and phthalic  
466 anhydride  $C_8H_5O_3^+$  ( $R=0.83$ ) are both known emissions from biomass burning aerosols (Brunns et al., 2017; Koss  
467 et al., 2018).  $C_6H_8O_5$  ( $R=0.84$ ) (Molteni et al., 2018) is an oxidation product of benzene, while  $C_7H_{10}O_6$  ( $R=0.84$ )  
468 as reported by Nakao et al. (Nakao et al., 2011), is an oxidation product of o-cresol, an emission from oxygenated  
469 aromatic BBOA. Therefore, we define this factor as mixed oxidized isoprene OA and BBOA.

470 The third factor was identified as BBOA due to its strong correlation ( $R=0.88$ ) with vanillic acid  $C_8H_8O_4$  (Fleming  
471 et al., 2020) and its prominent fragment ( $C_8H_6O_4$ ) with even higher correlation ( $R=0.96$ ), which constitutes a  
472 significant portion of this factor. Additionally, another BBOA tracer, syringic acid ( $C_9H_{10}O_5$ ) (Wan et al., 2019),  
473 and its fragment ( $C_9H_6O_3$ ,  $R=0.95$ ), likely formed by the loss of two  $H_2O$  molecules, or as a direct BBOA emission  
474 (Fleming et al., 2020), further support this identification. Other ions, such as  $C_6H_6O_5$  and  $C_7H_8O_5$ , are oxidation  
475 products of guaiacol (Yee et al., 2013). The diurnal cycle of this factor, peaking during the daytime, suggests that  
476 barbecue events may be contributing sources during the summer.

477 The fourth factor shows no correlation with other compounds and exhibits a distinct nighttime peak (Figure S10c).  
478 However, it correlates strongly with nitrate detected by AMS ( $R = 0.71$ ). This suggests that the factor represents  
479 regional background, with its nighttime increase likely influenced by local accumulation effects.

480 The fifth factor was identified as more oxidized monoterpene OA, comprising highly oxidized monoterpene  
481 products such as  $C_{10}H_{15}O_{3.5}^+$  ( $R=0.86, 0.85, 0.84$ ), diacetin  $C_7H_{13}O_5^+$  ( $R=0.79$ ), oxidized molecules of  
482 monoterpenes  $C_8H_{13}O_2^+$  ( $R=0.81$ ),  $C_8H_{13}O_4^+$  ( $R=0.80$ ), and its fragment ( $C_8H_{11}O_3^+$ ,  $R=0.83$ ). Compounds like  
483  $C_9H_{13}O_{3.4}^+$  ( $R=0.81, 0.78$ ) likely arise from fragments of the  $C_9H_{14}O_n$  series, representing more oxidized  
484 monoterpene products that have lost hydrogen. Compared to the diurnal pattern of less oxidized terpene products,  
485 this factor's peak displays a delay, suggesting that primary oxidation products form initially and then undergo  
486 further oxidation, resulting in more oxidized BOA (More OBOA).

487 In winter and spring, the first factor is identified as night-time aged BBOA due to the presence of distinct BBOA  
488 tracers,  $C_6H_6N_1O_4^+$  and  $C_7H_8N_1O_4^+$  (Figure S14a), which do not appear in the mass spectra of other factors.  
489 Nitrocatechols ( $C_6H_5N_1O_4$ ) originates from anthropogenic activities, including biomass burning and vehicle  
490 emissions. Meanwhile, methyl-nitrocatechols ( $C_7H_7N_1O_4$ ) are specific markers for BBOA, as they are formed  
491 from m-cresol released during biomass combustion and diesel exhaust (Kourtchev et al., 2016). These tracers also  
492 exhibit the same strong correlation of 0.97 with this factor (Table S8). Syringic acid ( $C_9H_{10}O_5$ ) also correlates  
493 well ( $R=0.70$ ) with this factor. In terms of its daily cycle did not show peaks during morning or evening rush  
494 hours; instead, a peak was observed around 8 p.m., suggesting it aligns more with BBOA. This factor showed a

495 strong correlation with highly oxidized nitrogen-containing compounds and secondary organic aerosols (syringic  
496 acid). This factor is more related to highly oxidized nitrogen-containing secondary organic aerosols, indicating  
497 that nitrogen-containing compounds produced by BBOA may have undergone significant oxidation by NO<sub>3</sub>  
498 radicals. Therefore, I identified it as night-time aged BBOA.

499 The second factor was characterized by a high fraction of oleic acid C<sub>18</sub>H<sub>35</sub>O<sub>2</sub><sup>+</sup> (R=0.90), C<sub>16</sub>H<sub>35</sub>O<sub>3</sub><sup>+</sup>  
500 (C<sub>16</sub>H<sub>33</sub>O<sub>2</sub>(H<sub>2</sub>O)<sup>+</sup>) (R=0.88), C<sub>16</sub>H<sub>33</sub>O<sub>2</sub><sup>+</sup> corresponding to palmitic acid (R=0.54), and C<sub>16</sub>H<sub>31</sub>O<sub>1</sub><sup>+</sup> is the fragment  
501 of C<sub>16</sub>H<sub>33</sub>O<sub>2</sub><sup>+</sup> (R=0.54). C<sub>18</sub>H<sub>34</sub>O<sub>2</sub> is identified as the cooking tracer oleic acid, while C<sub>16</sub>H<sub>33</sub>O<sub>2</sub><sup>+</sup> serves as another  
502 cooking aerosol tracer, corresponding to palmitic acid (Reyes-Villegas et al., 2018; Wang et al., 2020b; Huang et  
503 al., 2021). C<sub>16</sub>H<sub>31</sub>O<sub>1</sub><sup>+</sup> is thought to originate from C<sub>16</sub>H<sub>33</sub>O<sub>2</sub><sup>+</sup> due to fragmentation involving the loss of one H<sub>2</sub>O  
504 molecule. These findings strongly suggest that this factor represents cooking aerosol.

505 The third factor was identified as aged combustion. In this factor, the aromatic hydrocarbon C<sub>7</sub>H<sub>9</sub><sup>+</sup> accounts for a  
506 relatively higher fraction and exhibits a strong correlation (R = 0.79). Although C<sub>8</sub>H<sub>13</sub><sup>+</sup> does not contribute  
507 significantly as C<sub>7</sub>H<sub>9</sub><sup>+</sup>, it also shows the same strong correlation. These compounds are attributed to combustion  
508 sources (Wang et al., 2022). The ion C<sub>7</sub>H<sub>10</sub>N<sub>1</sub><sup>+</sup>, potentially a fragment of acridine (C<sub>7</sub>H<sub>12</sub>N<sub>1</sub><sup>+</sup>) originating from  
509 coal combustion (Wang et al., 2021), exhibits a distinct signal and the highest correlation (R = 0.94). Similarly,  
510 C<sub>6</sub>H<sub>15</sub>O<sub>3</sub><sup>+</sup> (R = 0.93) corresponds to 2-methoxyethyl ether (MXEE), a product of fuel combustion. Monoterpene  
511 oxidation products, such as C<sub>10</sub>H<sub>17</sub>O<sub>1</sub><sup>+</sup> (R = 0.86) and C<sub>9</sub>H<sub>13</sub>O<sub>1</sub><sup>+</sup> (R=0.82), are also observed. This is likely because  
512 monoterpenes, serving as biofuel components in engines and boilers, form oxidized monoterpene products when  
513 combusted and oxidized (Philippe Dagaut et al., 2024). Additionally, benzocaine C<sub>9</sub>H<sub>12</sub>N<sub>1</sub>O<sub>2</sub><sup>+</sup> exhibits strong  
514 correlation (R = 0.80) with this factor and is likely a product of oxidized combustion processes.

515 The fourth factor has C<sub>6</sub> carboxylic acids (C<sub>6</sub>H<sub>7</sub>O<sub>5</sub><sup>+</sup>) which is the phenol oxidation products with OH radicals in  
516 the low-NO<sub>x</sub> system, and C<sub>7</sub>H<sub>9</sub>O<sub>5</sub><sup>+</sup> denoted as the guaiacol with OH adduct. Propanedioic acid (C<sub>3</sub>H<sub>5</sub>O<sub>4</sub><sup>+</sup>),  
517 pentanedione (C<sub>4</sub>H<sub>5</sub>O<sub>3</sub><sup>+</sup>), and 2-oxopentanedioic acid C<sub>5</sub>H<sub>7</sub>O<sub>4</sub><sup>+</sup> are fragments derived from the OH oxidation  
518 products of biomass burning VOC (BBVOC) such as guaiacol and syringol (Yee et al., 2013). Additionally,  
519 C<sub>6</sub>H<sub>6</sub>O<sub>2</sub> is an OH radical oxidation product from phenol. A higher fraction of 2,5-di-(hydroxymethyl)furan  
520 C<sub>6</sub>H<sub>9</sub>O<sub>3</sub><sup>+</sup> was observed, which may result from C<sub>6</sub>H<sub>7</sub>O<sub>2</sub><sup>+</sup> binding with a water molecule. These photochemical  
521 products, formed from BBVOC oxidation by OH radicals, confirm that this factor represents aged BBOA. All the  
522 aforementioned ions exhibit a strong correlation of approximately 0.85 with this factor, as shown in Table S2.  
523 Furthermore, its diurnal pattern, with a peak at 15:00 during the day, leads to its identification as day-time aged  
524 BBOA.

525 The fifth factor shows a very strong correlation with stearic acid C<sub>18</sub>H<sub>37</sub>O<sub>2</sub><sup>+</sup> (R = 0.95), C<sub>16</sub>H<sub>33</sub>O<sub>2</sub>(H<sub>2</sub>O)<sup>+</sup> (R = 0.91),  
526 C<sub>18</sub>H<sub>15</sub>O<sub>1</sub><sup>+</sup> (R = 0.90), C<sub>19</sub>H<sub>15</sub>O<sub>1</sub><sup>+</sup> (R = 0.88), and oleic acid C<sub>18</sub>H<sub>35</sub>O<sub>2</sub><sup>+</sup> (R = 0.88). However, these compounds do  
527 not account for significant fractions in this factor's mass spectrum as they do in factor 2's mass spectrum. Notably,  
528 trimethoxy methane C<sub>4</sub>H<sub>11</sub>O<sub>3</sub><sup>+</sup> is a key ion in this factor but contributes minimally to others and shows no  
529 correlation with the factor (R = 0.02). While the composition includes unrelated compounds, its strong correlation  
530 with sulfate detected by AMS (R=0.74) suggests a regional background origin, with the nighttime peak indicating  
531 local accumulation effects.

532 During summer, the composition of SVOA includes 11 ± 15% weakly OBOA, 16 ± 15% oxidized isoprene &  
533 BBOA (mixture of oxidized isoprene OA and BBOA), 25 ± 21% BBOA, 30 ± 22% attributed to regional  
534 background sources, and 18 ± 16% to More OBOA (Figure 6). Although cooking-related SVOA ions were present

535 during summer, the higher contribution of biogenic oxidation products in overlapping mass spectral regions likely  
 536 reduced the statistical separability of a distinct cooking factor in the SVOC PMF analysis (Zhu et al., 2018;  
 537 Coggon et al., 2024a). In winter, nighttime aged BBOA accounts for  $10 \pm 9\%$ , cooking OA contributes  $4 \pm 5\%$ ,  
 538 aged combustion OA makes up  $9 \pm 10\%$ , daytime aged BBOA constitutes the largest fraction at  $55 \pm 21\%$ , and  
 539 regional background sources contribute  $23 \pm 17\%$ . In spring, nighttime aged BBOA accounts for  $12 \pm 12\%$ ,  
 540 cooking OA contributes  $11 \pm 12\%$ , aged combustion OA makes up  $24 \pm 18\%$ , daytime aged BBOA constitutes  
 541 the largest fraction at  $46 \pm 25\%$ , and regional background sources contribute  $7 \pm 9\%$ .

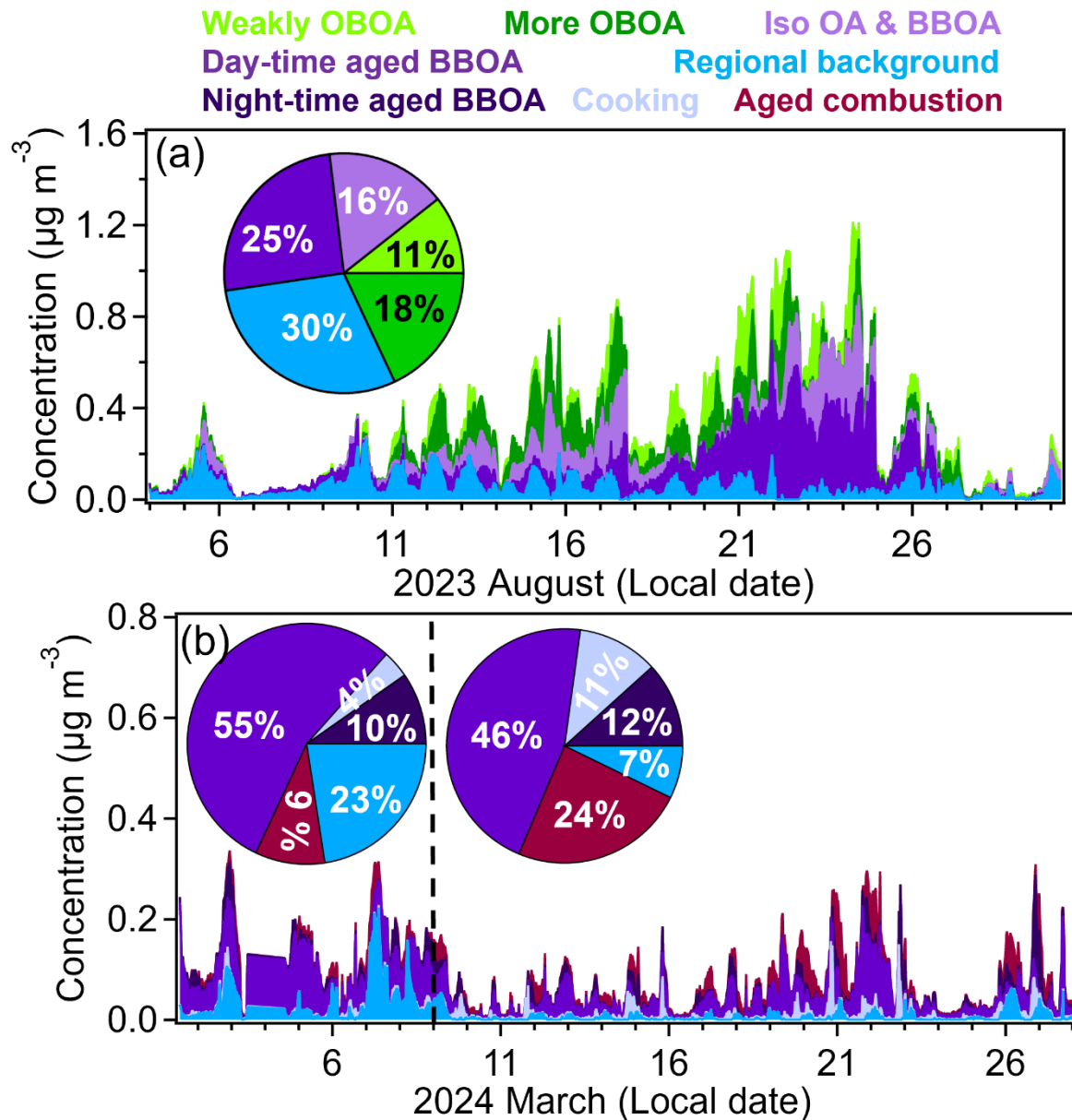


**Figure 6:** The time series and relative mass contributions (pie charts) of each SVOA factor to total SVOA concentrations in summer (a), winter (left of the dash line), and spring (right of the dash line) (b).

### 542 3.2.3 Sources of organic aerosol particles

543 This study thoroughly examined source factor profiles, diurnal patterns, and correlations with tracers (FigureS15-  
 544 16, S17-18, and S19-20) for OA particles. The average organic aerosol concentration was  $4.3 \pm 2.9 \mu\text{g m}^{-3}$  in  
 545 summer,  $3.4 \pm 1.7 \mu\text{g m}^{-3}$  in winter and  $1.8 \pm 1.8 \mu\text{g m}^{-3}$  in spring. Five OA factors were identified as the optimal

546 interpretable solutions for summer and winter/spring, respectively. Alternative PMF solutions with different factor  
547 numbers were systematically evaluated based on  $Q/Q_{\text{exp}}$  behavior, factor interpretability, and tracer correlations;  
548 details are provided in the Supplement (Figure S14).

549 In summer, the first factor was identified as cooking organic aerosol (COA), based on its high H: C ratio (1.82),  
550 low O: C ratio (0.19) (Figure S17a), higher contributions at  $m/z$  55 ( $\text{C}_3\text{H}_3\text{O}^+$ ) and  $m/z$  57 ( $\text{C}_3\text{H}_5\text{O}^+$ ), and the mass  
551 spectrum dominated by hydrocarbon ions. These characteristics are consistent with reported COA in urban areas  
552 (Elser et al., 2016; Äijälä et al., 2017; Liu et al., 2018). Additionally, fatty acid ( $\text{C}_{16}\text{H}_{35}\text{O}_3^+$ ) detected by  
553 CHARON-PTR showed a moderate correlation ( $R = 0.54$ ) with the COA time series (Figure 17b). The second  
554 factor is characterized by a mass spectrum also dominated by hydrocarbon ions, a similar O: C ratio, and a high  
555 O: C ratio, but with higher contributions at  $m/z$  55 ( $\text{C}_4\text{H}_7^+$ ) and  $m/z$  57 ( $\text{C}_4\text{H}_9^+$ ) (Elser et al., 2016). These features  
556 are consistent with the characteristics of hydrocarbon-like organic aerosol (HOA) which is related to traffic.  
557 additionally, HOA shows a good correlation ( $R= 0.66$ ) with the eBC time series. The third factor is assigned to  
558 Biogenic secondary organic aerosol (BOA), based on its H: C ratio of 1.63 and O: C of 0.44. The O/C ratio falls  
559 within the range typically associated with semi-volatile oxidized organic aerosol (SVOOA), which is  
560 approximately  $0.35 \pm 0.14$  (Setyan et al., 2012). And it has a good correlation of 0.86 with monoterpene oxidation  
561 products (pinonaldehyde) in CHARON-PTR. BOA's diurnal pattern (Figure S17c) shows an increase starting at  
562 8 pm, reaching its peak at 7 am. This trend aligns with the nighttime oxidation process of monoterpenes,  
563 supporting its identification as BOA. The fourth factor was identified as aged biomass burning organic aerosol  
564 (BBOA) because its O/C ratio of 0.597 is slightly higher than that of fresh BBOA (0.15-0.5) and falls within the  
565 range of aged BBOA (0.5-0.87) (Ortega et al., 2013). Its diurnal shows a small peak at 3 pm and a higher peak at  
566 10 pm, the nighttime peak indicates that fresh BBOA happened rapid dark aging process (Kodros et al., 2020).  
567 And it shows a strong correlation ( $R=0.93$ ) with BBOA tracer levoglucosan detected by CHARON-PTR. therefore,  
568 the fourth factor is identified as aged BBOA. The fifth factor has the lowest H: C ratio (1.43) and the highest O:C  
569 ratio 0.75, which falls within the range of low-volatility oxygenated organic aerosol (LVOOA) (0.6-1.0) (J. L.  
570 Jimenez et al., 2009). LVOOA is dominated by  $\text{CO}^+$  and  $\text{CO}_2^+$  and shows a strong correlation ( $R=0.70$ ) with  $\text{O}_3$ ,  
571 indicating that it is associated with photochemical oxidation processes (Kumar et al., 2016). Its diurnal pattern  
572 shows a daytime peak. These characteristics align well with the typical properties of LVOOA, leading to its  
573 identification as LVOOA. To ensure that every tracer detected by CHARON-PTR and correlated with AMS-PMF  
574 factors is representative, we compared different related fatty acids, toluene and trimethyl benzene, different  
575 monoterpene oxidation products, and different BBOA tracers. All of them showed good time-series correlations  
576 (Figure S19).

577 In winter, we identified all the factors using the same method as in summer. The difference is that the traffic  
578 diurnal cycle (Figure S18c) exhibits distinct peaks during the morning and evening rush hours. Fresh BBOA  
579 shows an evening peak, indicating evening residual heating activities. Aged BBOA is characterized by its  
580 correlation with  $\text{C}_6\text{H}_7\text{O}_5^+$ , which we identified as an oxidation product of BBOA in the CHARON-PTR section.  
581 its diurnal pattern is very flat, suggesting it may be associated with regional background levels or long-range  
582 transport. for LVOOA,  $\text{NH}_4^+$  is used as an indicator, as it correlates strongly with inorganic aerosol during autumn  
583 and winter (Freney et al., 2011). Other different OA factors time series shown in Figure S20.

584 In summer, OA contributions are as follows: traffic  $8 \pm 8\%$ , cooking  $11 \pm 13\%$ , BOA  $22 \pm 14\%$ , aged BBOA  $25$   
585  $\pm 21\%$ , and LVOOA  $33 \pm 20\%$ . In winter, the contributions are: traffic  $5 \pm 4\%$ , cooking  $12 \pm 12\%$ , fresh BBOA

586  $13 \pm 9\%$ , aged BBOA  $36 \pm 12\%$ , and LVOOA  $33 \pm 17\%$ . In spring, the contributions are: traffic  $9 \pm 7\%$ , cooking  
 587  $19 \pm 16\%$ , fresh BBOA  $27 \pm 17\%$ , aged BBOA  $37 \pm 19\%$ , and LVOOA  $9 \pm 10\%$  (Figure 7).

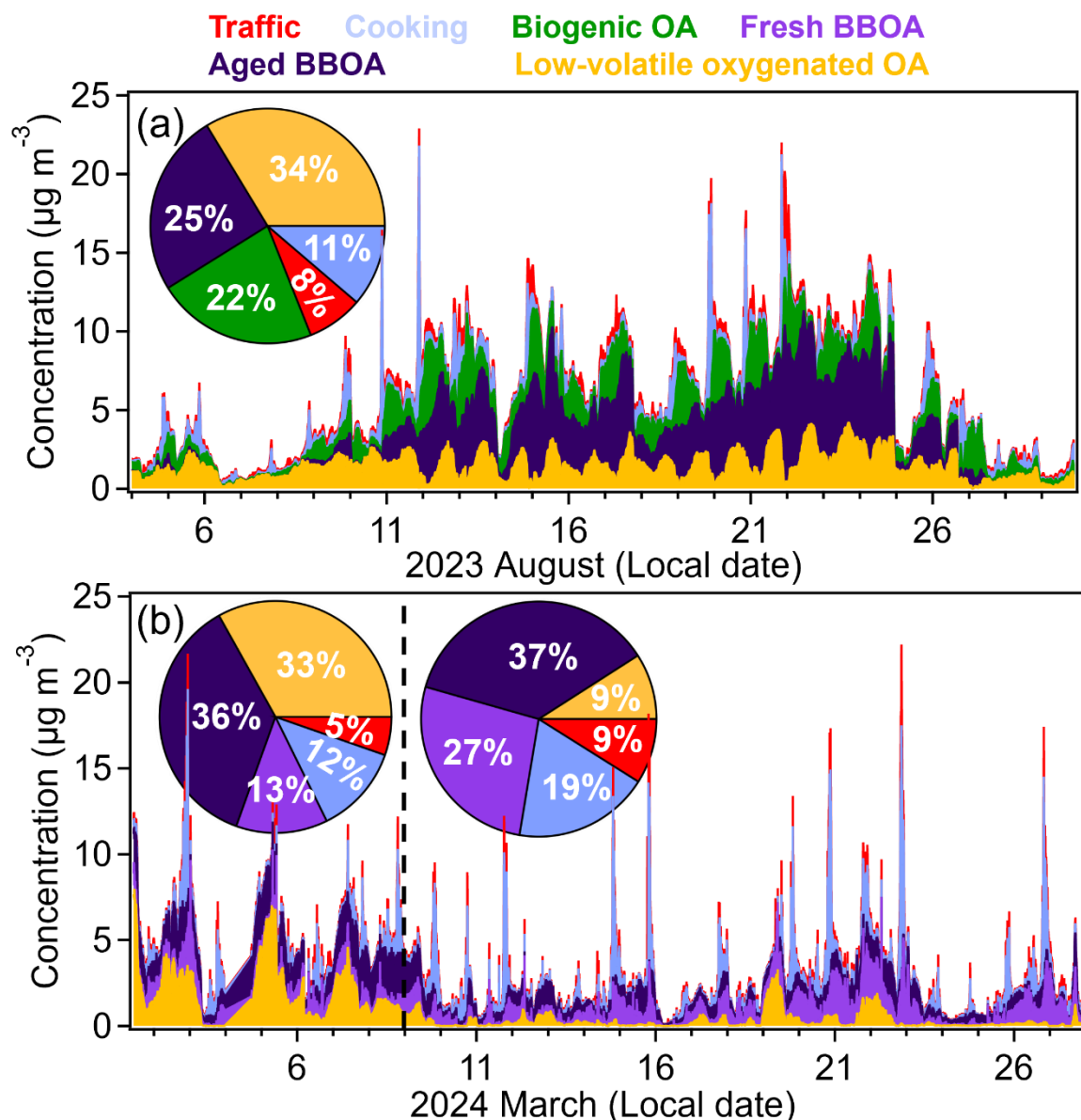


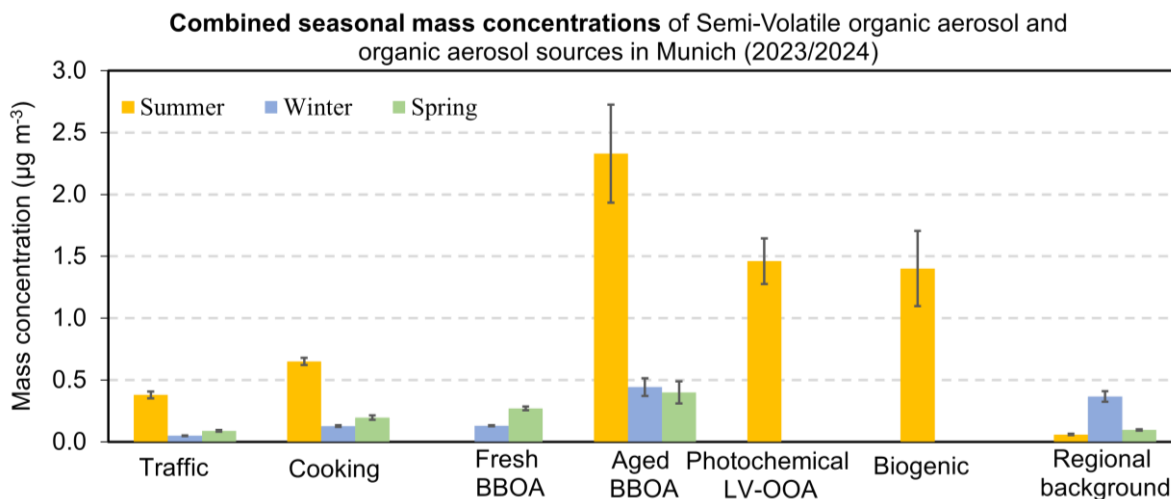
**Figure 7: The time series and relative mass contributions (pie charts) of each OA factor to total OA concentrations in summer (a), winter (left of the dash line), and spring (right of the dash line) (b).**

588  
 589 Previous PMF studies in Stuttgart and Karlsruhe identified consistent summer source patterns: traffic-related OA  
 590 contributes less than 10%, SV-OOA accounts for approximately 16%, while LV-OOA dominates at around 75%  
 591 of OA mass. This LV-OOA prevalence indicates strong biogenic influence from regional vegetation and  
 592 photochemical processes enhanced by higher summer temperatures. In Stuttgart, elevated winter  $\text{PM}_{2.5}$  stems  
 593 primarily from biomass burning and residential heating, evidenced by enhanced levoglucosan and nitrated phenol  
 594 signals, alongside increased traffic-related primary OA (POA). Both traffic OA and BBOA contribute  
 595 substantially, though LV-OOA remains significant. Karlsruhe experiences similar source patterns with increased  
 596 residential heating, traffic emissions, and coal combustion from industrial sources, but benefits from less severe  
 597 inversion and stagnation conditions, resulting in lower overall concentrations. Munich's intermediate winter

598 pollution levels suggest a source composition transitioning between these profiles, warranting detailed PMF  
 599 analysis to characterize its specific emission contributions and compare with the established patterns in Stuttgart  
 600 and Karlsruhe.

601 PMF source apportionment reveals strong seasonal dependencies in organic aerosol composition, with summer  
 602 conditions driving the majority of aerosol burden in Munich. Summer demonstrates the highest concentrations  
 603 across all source categories, dominated by aged BBOA ( $2.3 \mu\text{g m}^{-3}$ ) as the largest single contributor due to  
 604 barbecue charcoal combustion. Photochemical LV-OOA ( $1.5 \mu\text{g m}^{-3}$ ) and biogenic emissions ( $1.4 \mu\text{g m}^{-3}$ ) emerge  
 605 exclusively during summer, reflecting enhanced secondary aerosol formation under high temperatures and intense  
 606 solar radiation that promote both biogenic emissions and photochemical processing. In contrast, late winter and  
 607 spring show dramatically reduced organic aerosol levels, with late winter contributions limited primarily to  
 608 regional background ( $0.4 \mu\text{g m}^{-3}$ ) and minimal aged BBOA ( $0.4 \mu\text{g m}^{-3}$ ). Traffic and cooking emissions remain  
 609 consistently minor throughout all seasons ( $\leq 0.7 \mu\text{g m}^{-3}$ ), suggesting these local primary sources are less  
 610 significant compared to secondary formation processes and regional biomass burning influences.

611 SVOA and OA composition exhibits distinct seasonal patterns driven by varying source emissions and  
 612 atmospheric processing. Summer periods show elevated OA concentrations due to enhanced photochemical  
 613 oxidation under high solar radiation, promoting secondary organic aerosol formation (Figure 8). Biogenic sources  
 614 contribute significantly during summer through increased vegetation emissions. Rapid atmospheric oxidation  
 615 transforms fresh BBOA to aged BBOA, explaining the predominance of aged BBOA despite active barbecue  
 616 activities. In late winter, residential heating dominated fresh BBOA emissions. During early spring, both heating  
 617 and barbecue emissions contributed to fresh BBOA, with the latter increasing as temperatures rose. Consequently,  
 618 Fresh BBOA concentrations increased from late winter to early spring. However, Fresh BBOA became less  
 619 detectable in peak summer due to accelerated aging processes under higher temperatures and enhanced  
 620 photochemical activity. Late winter and spring show substantial aged BBOA from residential heating activities.  
 621 Cooking and traffic emissions remain consistent year-round sources, though their oxidation efficiency increases  
 622 significantly in summer compared to winter and early spring when photochemical processes are less active.



623  
 624 **Figure 8: Comprehensive seasonal mass contributions of SVOA and OA sources in Munich summer, winter and spring**  
 625 **time (Source categories combine factors from Charon-PTR-MS and HR-TOF-AMS: Aged BBOA (day-time aged**  
 626 **BBOA, night-time aged BBOA, and IsoOA & BBOA from Charon; aged BBOA from AMS), Biogenic OA (weakly**  
 627 **OBOA and More OBOA from Charon; BOA from AMS), with remaining sources combined similarly). Please note,**  
 628 **that the total OA concentrations were  $4.3 \pm 2.9 \mu\text{g m}^{-3}$  in summer,  $3.4 \pm 1.7 \mu\text{g m}^{-3}$  in winter, and  $1.8 \pm 1.8 \mu\text{g m}^{-3}$  in**  
 629 **spring.**

### 630 3.3 Seasonal strong biomass burning aerosol events

631 PMF analysis of AMS mass spectra reveals that aged BBOA substantially contributes to total OA with seasonal  
632 variations:  $25 \pm 21\%$  in summer,  $36 \pm 12\%$  in winter, and  $37 \pm 19\%$  in spring. Two prominent BBOA events were  
633 observed during August 22<sup>nd</sup>-24<sup>th</sup> (OA:  $7.9 \pm 1.7 \mu\text{g m}^{-3}$ ) and March 7<sup>th</sup>-9<sup>th</sup> (OA:  $3.3 \pm 1.3 \mu\text{g m}^{-3}$ ).

634 During August 2023, aged BBOA showed strong correlations with multiple biomass burning indicators (Figure 9  
635 and Table S10). The high correlation with eBC ( $R=0.75$ ) suggests significant light-absorbing carbon from  
636 combustion processes. Primary biomass burning tracers showed excellent correlations: levoglucosan ( $\text{C}_6\text{H}_{11}\text{O}_5^+$ ,  
637  $R=0.93$ ) and syringic acid ( $\text{C}_9\text{H}_{11}\text{O}_5^+$ ,  $R=0.84$ ), confirming fresh biomass burning emissions. The strong  
638 correlation with atmospheric oxidation products such as  $\text{C}_6\text{H}_7\text{O}_5^+$  ( $R=0.88$ , phenol oxidation products from OH  
639 radical reactions under low- $\text{NO}_x$  conditions) and  $\text{C}_7\text{H}_9\text{O}_5^+$  ( $R=0.87$ , guaiacol-OH oxidation products) indicates  
640 significant photochemical aging processes during summer. Notably, aged BBOA correlated strongly with  
641 barbecue charcoal combustion tracers including formaldehyde ( $R=0.80$ ) (Kabir et al., 2010), coniferyl alcohol  
642 ( $\text{C}_{10}\text{H}_{13}\text{O}_3^+$ ,  $R=0.90$ ), pinic acid ( $\text{C}_9\text{H}_{15}\text{O}_4^+$ ,  $R=0.76$ ), and homovanilic acid ( $\text{C}_9\text{H}_{11}\text{O}_4^+$ ,  $R = 0.83$ ) (Vicente et al.,  
643 2018). Several of these tracers are considered more specific to charcoal combustion than to traffic or fossil-fuel  
644 sources, and the pronounced evening maximum of the factor is consistent with typical barbecue activity patterns,  
645 supporting a local grilling-related origin. Backward trajectory analysis combined with VIIRS fire radiative power  
646 (FRP) data for August suggests negligible influence from regional wildfires along the air-mass transport pathways  
647 (Fig. S21a). Although several fire detections classified as “unknown” sources were observed (Fig. S21b), their  
648 FRP values were very low, indicating weak fire intensity and suggesting that they are unlikely to contribute  
649 substantially to the elevated BBOA levels observed in Munich. However, during the intensive BBOA episode  
650 (August 22<sup>nd</sup>-24<sup>th</sup>), most tracer correlations decreased slightly, and formaldehyde showed no correlation with aged  
651 BBOA ( $R= -0.20$ ) in Table S10. This suggests that during high-concentration events, different source  
652 contributions alter the chemical fingerprint, possibly indicating the influence of additional fresh emissions or  
653 changes in atmospheric processing conditions. Back trajectory analysis during the strong BBOA event shows that  
654 51% of air masses originated from long-range transport near the Belgium border (average BBOA:  $5.3 \mu\text{g m}^{-3}$ ),  
655 while 15% from the Bavarian region exhibited the highest concentrations ( $7.3 \mu\text{g m}^{-3}$ ) in Figure S22. Given the  
656 absence of wildfire sources and the strong correlations with barbecue charcoal combustion tracers, we attribute  
657 the elevated concentrations primarily to outdoor barbecue charcoal combustion emissions.

658 In the whole March 2024, aged BBOA exhibited markedly different correlation patterns, indicating distinct  
659 sources and processes. The weaker correlation with eBC ( $R=0.39$ ) suggests different combustion characteristics  
660 compared to summer. Most importantly, aged BBOA showed poor correlations with barbecue charcoal  
661 combustion tracers: formaldehyde ( $R=0.14$ ), coniferyl alcohol ( $R=0.47$ ), pinic acid ( $R=0.41$ ), and homovanilic  
662 acid ( $R=0.51$ ). The dramatic decrease in these correlations compared to summer values indicate minimal  
663 contribution from outdoor cooking activities during winter months. Primary biomass burning markers also showed  
664 reduced correlations: levoglucosan ( $R=0.30$ ), and syringic acid ( $\text{C}_9\text{H}_{11}\text{O}_5^+$ ,  $R=0.24$ ), suggesting different emission  
665 sources or processing pathways. Conversely, aged BBOA maintained strong correlations with guaiacol oxidation  
666 products:  $\text{C}_6\text{H}_7\text{O}_5^+$  ( $R=0.80$ ) and  $\text{C}_7\text{H}_9\text{O}_5^+$  ( $R=0.74$ ). This pattern strongly indicates that winter aged BBOA  
667 primarily originates from residential heating emissions that have undergone atmospheric oxidation (Kodros et al.,  
668 2020). The guaiacol derivatives are characteristic markers of wood combustion for heating purposes, and their

669 predominant correlations with aged BBOA confirm this source attribution. In contrast, fresh BBOA showed strong  
670 correlations with barbecue charcoal combustion tracers: coniferyl alcohol ( $R=0.69$ ), pinic acid ( $R=0.68$ ), and  
671 homovanilic acid ( $R=0.67$ ), as well as primary biomass burning markers including levoglucosan ( $R=0.72$ ) and  
672 syringic acid ( $R=0.62$ ). Notably, fresh BBOA showed weak correlation with the aged oxidation products ( $C_6H_7O_5^+$   
673 and  $C_7H_9O_5^+$ ) that strongly correlated with aged BBOA. This divergent correlation pattern suggests that fresh  
674 BBOA during late winter and early spring is associated with primary biomass-burning emissions, likely dominated  
675 by residential heating under weak photochemical conditions, with additional contributions from barbecue charcoal  
676 combustion as temperatures increase. Because these sources share similar biomass-burning signatures, a  
677 separation between residential heating and barbecue emissions has significant uncertainty. The observed  
678 separation between fresh and aged BBOA characteristics reflects slower atmospheric aging during colder periods  
679 compared to summer conditions, resulting in a clear separation between fresh and aged BBOA characteristics.

680 The intensive episode analysis (March 7<sup>th</sup>-9<sup>th</sup>, 2024) revealed correlation patterns consistent with the monthly  
681 analysis (Table S10), reinforcing the conclusion that seasonal BBOA sources shift from barbecue charcoal  
682 combustions in summer to residential heating in winter. During this episode, aged BBOA maintained strong  
683 correlations exclusively with guaiacol oxidation products ( $C_6H_7O_5^+$  and  $C_7H_9O_5^+$ ), consistent with the monthly  
684 pattern. However, fresh BBOA exhibited notably selective correlations, showing moderate relationships only with  
685 coniferyl alcohol ( $R=0.65$ ) and levoglucosan ( $R=0.62$ ), while displaying weak or negligible correlations with  
686 other tracers. The limited correlation pattern of fresh BBOA can be attributed to its substantially lower  
687 concentration compared to aged BBOA during this period (Table S10). When aged BBOA dominates the total  
688 BBOA mass, the temporal variability of most tracers is primarily governed by the aged component, effectively  
689 masking the correlation signals from fresh BBOA. As a minor constituent, fresh BBOA's true relationships with  
690 various tracers become statistically obscured, making it challenging to establish robust correlations beyond the  
691 most characteristic primary emission markers (i.e., levoglucosan and coniferyl alcohol). This phenomenon  
692 highlights the importance of aged BBOA as the dominant source during winter heating periods, while fresh  
693 emissions represent localized, transient contributions that are rapidly diluted within the regional aged aerosol  
694 background. Back trajectory analysis reveals distinctly different transport patterns compared to summer. Winter  
695 air masses predominantly followed three clusters: Cluster 1 (32%) transported through Czechia with BBOA  
696 concentrations of  $2.3 \mu\text{g m}^{-3}$ , Cluster 2 (14%) originating from Poland passing through Czechia ( $1.8 \mu\text{g m}^{-3}$ ), and  
697 Cluster 3 (19%) from the Belarus-Poland border passing through Czechia and Austria ( $1.1 \mu\text{g m}^{-3}$ ) in Figure S22.  
698 The dominance of Czechia-influenced trajectories (65%) contrasts sharply with summer patterns, indicating  
699 significant contributions from Central European residential heating emissions. The prevalence of aged BBOA in  
700 these air masses suggests substantial accumulation of Aged BBOA during long-range transport. Notably, Cluster  
701 2 exhibited elevated fresh BBOA concentrations, evidenced by lower O:C ratios, indicating recent biomass  
702 burning emissions from residential heating activities along the Polish transport pathway.

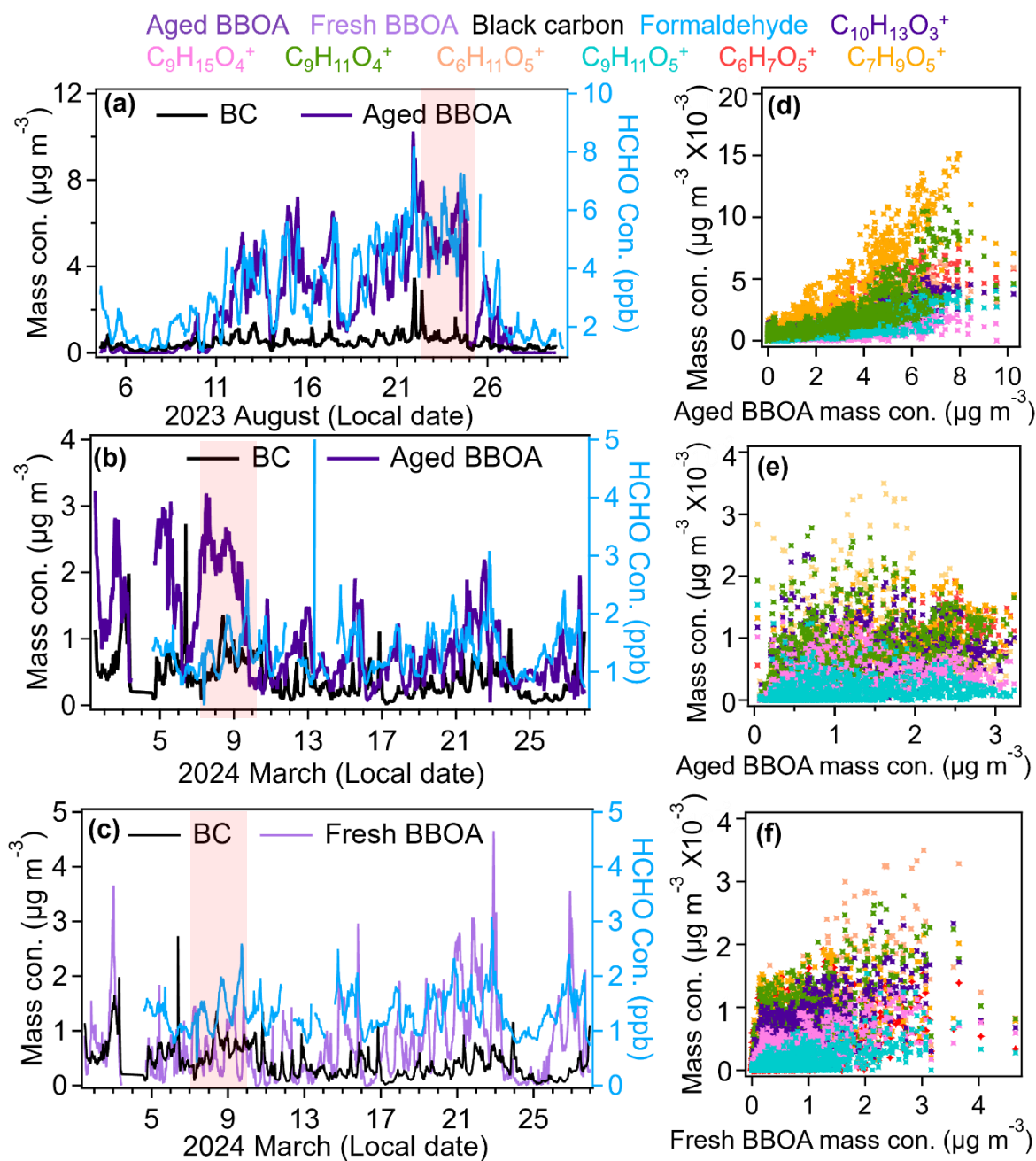


Figure 9. Time series of aged BBOA, black carbon, and formaldehyde during summer (August 2023, a) and winter/spring (March 2024, b) periods and fresh BBOA during March 2024 (c); Scatter plots showing correlations between aged BBOA and barbecue charcoal combustion tracers ( $C_{10}H_{13}O_3^+$ ,  $C_9H_{15}O_4^+$ ,  $C_9H_{11}O_4^+$ ), and biomass burning tracers ( $C_6H_{11}O_5^+$ ,  $C_9H_{11}O_5^+$ ,  $C_9H_7O_3^+$ ,  $C_6H_7O_5^+$ ,  $C_7H_9O_5^+$ ) in summer (d), in winter (e) and Fresh BBOA correlated with all the tracers (f). Strong BBOA events are in red shade.

#### 703 4. Conclusions

704 This study investigates the sources, concentrations, and seasonal variations of VOC, SVOA, and OA in an urban  
 705 street canyon of the third largest German city, Munich, using a combination of online mass spectrometric  
 706 observations and PMF based source apportionment. The results reveal a complex interplay between anthropogenic  
 707 and biogenic sources, as well as atmospheric photochemical aging that governs the composition and evolution of  
 708 the atmospheric pollutants in the urban street canyon.

709 The PM<sub>2.5</sub> analysis reveals Munich's distinctive air quality profile for different seasons. During summer, Munich's  
710 PM<sub>2.5</sub> concentrations ( $6.7 \pm 3.7 \mu\text{g m}^{-3}$ ) are comparable to neighboring German cities like Stuttgart ( $7.1 \pm 3.3 \mu\text{g}$   
711  $\text{m}^{-3}$ ) and Karlsruhe ( $7.0 \pm 3.5 \mu\text{g m}^{-3}$ ), also reflecting similar regional background conditions. Winter shows  
712 greater divergence: Munich's levels ( $13.0 \pm 7.4 \mu\text{g m}^{-3}$ ) exceed Karlsruhe's ( $5.6 \pm 4.9 \mu\text{g m}^{-3}$ ) but remain  
713 substantially lower than Stuttgart's pollution ( $27.0 \pm 11.9 \mu\text{g m}^{-3}$ ) also caused by stronger industrial sources in a  
714 basin like topography (Huang et al., 2019). This intermediate profile becomes even more significant when  
715 considering Munich's status as Germany's third-largest city, with a dense urban population and strong economic  
716 activity generating complex emission patterns, however, with less classical emissions from heavy  
717 industry. Compared to other European cities - Paris with winter PM<sub>2.5</sub> maximum of  $15 \mu\text{g m}^{-3}$ , Berlin's winter PM<sub>2.5</sub>  
718 episodes above  $15 \mu\text{g m}^{-3}$  (the World Health Organization (2021) recommended daily limit), or Bern's winter  $14$   
719  $\mu\text{g m}^{-3}$  average (Bressi et al., 2013; Grange et al., 2021; Renard et al., 2024) - Munich represents a critical test  
720 case with high population density, thriving industries and tourism.

721 Our findings identify and quantify a pronounced seasonal regime shift in organic aerosol composition. While a  
722 substantial anthropogenic baseline from traffic is persistent, the system transitions from a winter regime  
723 dominated by primary biomass burning aerosols (BBOA contributing up to 64% of OA) to a summer regime  
724 governed by photochemical aging (LVOOA at 33%) and formation of secondary biogenic aerosol. Critically, we  
725 demonstrate that biomass burning is not confined to the heating season. The significant and rising contribution  
726 from barbecue emissions in spring and summer reveals an underappreciated, health-sensitive emission source  
727 (Lenssen et al., 2022; Xu et al., 2023; Gruber and Kalamas, 2024).

728 The seasonal evolution of BBOA provides critical insights into its atmospheric processing. The presence of both  
729 fresh and aged BBOA in winter (fresh:  $13 \pm 9\%$ ; aged:  $36 \pm 12\%$ ) and spring (fresh:  $27 \pm 17\%$ ; aged:  $37 \pm 19\%$ )  
730 contrasts sharply with the aerosol composition in summer, where only aged BBOA ( $25 \pm 21\%$ ) is detected. This  
731 pattern strongly indicates that primary biomass burning emissions undergo rapid atmospheric oxidation in summer,  
732 with substantial conversion to the aged type driven by enhanced photochemical activity (e.g., higher temperatures,  
733 radiation, and O<sub>3</sub> levels). This rapid aging process for BBOA (Kodros et al., 2020; Li et al., 2023) presents a  
734 marked contrast to the typically slower, multi-generational oxidation pathway of anthropogenic VOCs from traffic  
735 (Srivastava et al., 2022), which require substantial atmospheric processing to form condensable SOA. A key  
736 implication of this finding is that if biomass burning OA persists in the atmosphere despite rapid aging processes,  
737 then mitigation strategies targeting primary biomass burning emissions could yield more immediate air quality  
738 benefits. We identified nocturnal oxidation of biogenic VOC as a significant SOA formation pathway in summer.

739 The substantial contribution of biogenic VOCs (oxidized BVOC:  $13 \pm 13\%$ , and BVOC:  $7 \pm 7\%$ ), coupled with  
740 BOA from oxidized monoterpenes ( $22 \pm 14\%$ ), demonstrates that nocturnal oxidation (primarily by O<sub>3</sub> and NO<sub>3</sub>  
741 radicals) generates secondary aerosol yields comparable those from daytime photochemical production (e.g.,  
742 LVOOA at  $33 \pm 20\%$ ). Consequently, monoterpene emission profiles must be treated as a critical air quality  
743 parameter and considered in urban vegetation management (Ren et al., 2014). It should be taken into account that  
744 the urban green can have positive but also negative impact on the levels of aerosol particles. Urban green  
745 infrastructure provides multiple environmental and health benefits, but may also influence secondary aerosol and  
746 ozone formation depending on species-specific BVOC emission characteristics (Ahn et al., 2022; Wang et al.,  
747 2025; Ma et al., 2025). For example, urban forestry programs can preferentially plant lower-monoterpene-emitting  
748 species such as *Ginkgo biloba* or *Taxus cuspidata* instead of high-emitting conifers such as *Metasequoia*

749 glyptostroboides in NO<sub>x</sub>-rich street canyons, or adjust pruning and replacement strategies accordingly, which may  
750 help balance air-quality impacts while preserving ecosystem benefits (Maison et al., 2024).

751 Previous studies in Stuttgart and Karlsruhe (Huang et al., 2019; Song et al., 2022; Zhang et al., 2024) identified  
752 traffic-related OA contributions consistently at or below 10% during summer. Munich exhibits similar patterns,  
753 with traffic OA contributing  $8 \pm 8\%$  in summer,  $5 \pm 4\%$  in winter, and  $9 \pm 7\%$  in spring. This consistency across  
754 all three cities in southwest Germany indicates that traffic is a minor OA component, exhibiting only relatively  
755 small seasonal variations. The most significant difference emerges in the abundance of LV-OOA. In Stuttgart and  
756 Karlsruhe, LV-OOA dominates summer OA with approximately 75%, reflecting strong biogenic influence from  
757 regional vegetation and photochemical processes enhanced by higher temperatures. In contrast, Munich's LV-  
758 OOA remains substantially lower and relatively stable for different seasons ( $33 \pm 20\%$  summer,  $33 \pm 17\%$  winter,  
759  $9 \pm 10\%$  spring), indicating either reduced biogenic precursor emissions or weaker photochemical oxidation  
760 despite comparable regional conditions. In Stuttgart, elevated winter PM<sub>2.5</sub> stems primarily from biomass burning  
761 and residential heating, evidenced by enhanced levoglucosan and nitrated phenol signals. Both traffic OA and  
762 BBOA contribute substantially to winter pollution. Karlsruhe exhibits similar patterns, with residential heating,  
763 traffic emissions, and coal combustion from industrial sources driving winter PM<sub>2.5</sub> increases. Munich's source  
764 profile diverges markedly from both cities. BBOA contributes substantially more to Munich's OA composition  
765 year-round compared to Stuttgart and Karlsruhe. Summer shows notable BBOA contribution (aged BBOA  $25 \pm$   
766  $21\%$  combined with BOA  $22 \pm 14\%$ ), and winter BBOA dominance increases dramatically (fresh BBOA  $13 \pm 9\%$   
767 plus aged BBOA  $36 \pm 12\%$ ). Spring displays the highest BBOA contribution (fresh BBOA  $27 \pm 17\%$  plus aged  
768 BBOA  $37 \pm 19\%$ ), indicating sustained biomass burning influence extending beyond residential heating into  
769 recreational activities. This persistent, elevated BBOA signature distinguishes Munich as a BBOA-dominated  
770 system, contrasting with the LV-OOA-dominated profiles of Stuttgart and Karlsruhe, and suggests that biomass  
771 burning requires year-round mitigation strategies in Munich.

772 In summary, this work reveals the dynamic chemical evolution of urban aerosol. The interplay between primary  
773 emissions from heating and cooking, the relatively constant traffic baseline, and the seasonally-modulated  
774 photochemical and nocturnal monoterpene chemistry creates a complex but decipherable pollution phenotype.  
775 Future research should prioritize tracking the atmospheric evolution of key source markers (e.g., from barbecues  
776 especially in summer and spring) to constrain their aging timescales and health-relevant properties. Integrating  
777 these process-level insights is paramount for refining air quality models like PALM-4U (Zhang et al., 2024; Resler  
778 et al., 2024; Samad et al., 2024) to accurately predict effectivity of measures to improve air quality in future urban  
779 scenarios.

#### 780 **Conflict of interests statement:**

781 Two co-authors are co-editors of ACP but the authors declare that there is no conflict of interests.

#### 782 **Author contributions**

783 FK, JC, and HS conceived the concept, planned, and organized the campaign. YXL did the AMS and PTR-MS  
784 measurements, analyzed most of the data and wrote the manuscript with contributions from all co-authors. HS  
785 planned and organized the measurements, took care of the particle number, size and additional trace gas

786 measurements. HZ, SA, AW, JC and FK supported instrument set up and conducted lidar measurements. XS,  
787 YWL and FK checked and calibrated the instruments during the measurements. JBS, ZA, and JS contributed to  
788 data analysis. TL contributed to planning of the measurement campaign and reviewed the manuscript.

#### 789 **Data availability**

790 The data used in this study is available at the KIT data repository KITopen data (DOI:10.35097/bs139dd72  
791 d5s0r6a).

#### 792 **Acknowledgement**

793 We gratefully acknowledge the support by the meteorological department of the Ludwig-Maximilians-University  
794 of Munich (Group of Prof. Bernhard Mayer) and especially Markus Garhammer. The support by the technical  
795 team (Group of Steffen Vogt) of the Institute of Meteorology and Climate Research Atmospheric Aerosol  
796 Research of the Karlsruhe Institute of Technology was extremely helpful.

#### 797 **Funding**

798 The China Scholarship Council (CSC) provided PhD scholarships for Yanxia Li and Xuefeng Shi. The KIT  
799 Graduate School for Climate and Environment (GRACE) supported Yanxia Li. The KIT funded the campaign in  
800 the program “Changing Earth – Sustaining our Future” of the Helmholtz Association. The campaign was partly  
801 funded by the Institute for Advanced Study, Technical University of Munich (Grant no. 291763). The TUM  
802 authors are partly supported by ERC Consolidator Grant CoSense4Climate (Grant 101089203) and Bavarian State  
803 Ministry of the Environment (Grant TLK 01U-75487). Yaowei Li acknowledges partial support from the NOAA  
804 Climate and Global Change Postdoctoral Fellowship Program, administered by UCAR's Cooperative Programs  
805 for the Advancement of Earth System Science (CPAESS) under award #NA23OAR4310383B.

#### 806 **5. References**

- 807 Ahn, J.-W., Dinh, T.-V., Park, S.-Y., Choi, I.-Y., Park, C.-R., and Son, Y.-S.: Characteristics of biogenic volatile  
808 organic compounds emitted from major species of street trees and urban forests, *Atmospheric Pollution*  
809 *Research*, 13, 10.1016/j.apr.2022.101470, 2022.
- 810 Äijälä, M., Daellenbach, K. R., Canonaco, F., Heikkinen, L., Junninen, H., Petäjä, T., Kulmala, M., Prévôt, A. S.  
811 H., and Ehn, M.: Constructing a data-driven receptor model for organic and inorganic aerosol – a synthesis  
812 analysis of eight mass spectrometric data sets from a boreal forest site, *Atmos. Chem. Phys.*, 19, 3645-3672,  
813 10.5194/acp-19-3645-2019, 2019.
- 814 Äijälä, M., Heikkinen, L., Fröhlich, R., Canonaco, F., Prévôt, A. S. H., Junninen, H., Petäjä, T., Kulmala, M.,  
815 Worsnop, D., and Ehn, M.: Resolving anthropogenic aerosol pollution types – deconvolution and exploratory  
816 classification of pollution events, *Atmospheric Chemistry and Physics*, 17, 3165-3197, 10.5194/acp-17-3165-  
817 2017, 2017.
- 818 Allison C. Aiken, Peter F. DeCarlo, Jesse H. Kroll, Douglas R. Worsnop, J. Alex Huffman, Kenneth S. Docherty,  
819 Ingrid M. Ulbrich, Claudia Mohr, Joel R. Kimmel, Donna Sueper, Yele Sun, Qi Zhang, Achim Trimborn,

820 Megan Northway, Paul J. Ziemann, Manjula R. Canagaratna, Timothy B. Onasch, M. Rami Alfarra, and Prevot,  
821 A. S. H.: O/C and OM/OC Ratios of Primary, Secondary, and Ambient Organic Aerosols with High-  
822 Resolution Time-of-Flight Aerosol Mass Spectrometry, *Environmental Science & Technology*, 42, 4478-4485,  
823 2008.

824 Messwertarchiv - LfU Bayern: <https://www.lfu.bayern.de/luft/immissionsmessungen/messwertarchiv/index.htm>,  
825 last access: 29.09.

826 Belis, C. A., Larsen, B. R., Amato, F., El Haddad, I., Favez, O., Harrison, R. M., Hopke, P. K., Nava, S., Paatero,  
827 P., Prévôt, A., Quass, U., Vecchi, R., and Viana, M.: European Guide on Air Pollution Source Apportionment  
828 with Receptor Models, European Commission, Joint Research Centre, Institute for Environment and  
829 Sustainability, Luxembourg: Publications Office of the European Union, 10.2788/9307, 2013.

830 Borbon, A., Herve, F., Marc, V., Nadine, L., J.C., G., and Renle, G.: An investigation into the traffic-related  
831 fraction of isoprene at an urban location, *Atmospheric Environment*, 35, 3749–3760, 2001.

832 Bressi, M., Sciare, J., Gherzi, V., Bonnaire, N., Nicolas, J. B., Petit, J. E., Moukhtar, S., Rosso, A., Mihalopoulos,  
833 N., and Féron, A.: A one-year comprehensive chemical characterisation of fine aerosol (PM<sub>2.5</sub>) at urban,  
834 suburban and rural background sites in the region of Paris (France), *Atmos. Chem. Phys.*, 13, 7825-7844,  
835 10.5194/acp-13-7825-2013, 2013.

836 Bruns, E. A., Slowik, J. G., El Haddad, I., Kilic, D., Klein, F., Dommen, J., Temime-Roussel, B., Marchand, N.,  
837 Baltensperger, U., and Prévôt, A. S. H.: Characterization of gas-phase organics using proton transfer reaction  
838 time-of-flight mass spectrometry: fresh and aged residential wood combustion emissions, *Atmospheric  
839 Chemistry and Physics*, 17, 705-720, 10.5194/acp-17-705-2017, 2017.

840 Canagaratna, M. R., Jimenez, J. L., Kroll, J. H., Chen, Q., Kessler, S. H., Massoli, P., Hildebrandt Ruiz, L., Fortner,  
841 E., Williams, L. R., Wilson, K. R., Surratt, J. D., Donahue, N. M., Jayne, J. T., and Worsnop, D. R.: Elemental  
842 ratio measurements of organic compounds using aerosol mass spectrometry: characterization, improved  
843 calibration, and implications, *Atmospheric Chemistry and Physics*, 15, 253-272, 10.5194/acp-15-253-2015,  
844 2015.

845 Canagaratna, M. R., Jayne, J. T., Jimenez, J. L., Allan, J. D., Alfarra, M. R., Zhang, Q., Onasch, T. B., Drewnick,  
846 F., Coe, H., Middlebrook, A., Delia, A., Williams, L. R., Trimborn, A. M., Northway, M. J., DeCarlo, P. F.,  
847 Kolb, C. E., Davidovits, P., and Worsnop, D. R.: Chemical and microphysical characterization of ambient  
848 aerosols with the aerodyne aerosol mass spectrometer, *Mass Spectrom Rev*, 26, 185-222, 10.1002/mas.20115,  
849 2007.

850 Chakraborty, A., Tripathi, S. N., and Gupta, T.: Effects of organic aerosol loading and fog processing on organic  
851 aerosol volatility, *Journal of Aerosol Science*, 105, 73-83, 10.1016/j.jaerosci.2016.11.015, 2017.

852 Chen, G., Canonaco, F., Slowik, J. G., Daellenbach, K. R., Tobler, A., Petit, J. E., Favez, O., Stavroulas, I.,  
853 Mihalopoulos, N., Gerasopoulos, E., El Haddad, I., Baltensperger, U., and Prevot, A. S. H.: Real-Time Source  
854 Apportionment of Organic Aerosols in Three European Cities, *Environ Sci Technol*, 56, 15290-15297,  
855 10.1021/acs.est.2c02509, 2022a.

856 Chen, G., Canonaco, F., Tobler, A., Aas, W., Alastuey, A., Allan, J., Atabakhsh, S., Aurela, M., Baltensperger,  
857 U., Bougiatioti, A., De Brito, J. F., Ceburnis, D., Chazeau, B., Chebaicheb, H., Daellenbach, K. R., Ehn, M.,  
858 El Haddad, I., Eleftheriadis, K., Favez, O., Flentje, H., Font, A., Fossun, K., Freney, E., Gini, M., Green, D.  
859 C., Heikkinen, L., Herrmann, H., Kalogridis, A. C., Keernik, H., Lhotka, R., Lin, C., Lunder, C., Maasikmets,

860 M., Manousakas, M. I., Marchand, N., Marin, C., Marmureanu, L., Mihalopoulos, N., Mocnik, G., Necki, J.,  
861 O'Dowd, C., Ovadnevaite, J., Peter, T., Petit, J. E., Pikridas, M., Matthew Platt, S., Pokorna, P., Poulain, L.,  
862 Priestman, M., Riffault, V., Rinaldi, M., Rozanski, K., Schwarz, J., Sciare, J., Simon, L., Skiba, A., Slowik, J.  
863 G., Sosedova, Y., Stavroulas, I., Styszko, K., Teinmaa, E., Timonen, H., Tremper, A., Vasilescu, J., Via, M.,  
864 Vodicka, P., Wiedensohler, A., Zografou, O., Cruz Minguillon, M., and Prevot, A. S. H.: European aerosol  
865 phenomenology - 8: Harmonised source apportionment of organic aerosol using 22 Year-long ACSM/AMS  
866 datasets, *Environ Int*, 166, 107325, [10.1016/j.envint.2022.107325](https://doi.org/10.1016/j.envint.2022.107325), 2022b.

867 Dense Air Quality Sensor Network: <https://www.ee.cit.tum.de/esm/projekte/dense-air-quality-sensor-network/>,  
868 last access: 17 October.

869 Coggon, M. M., Stockwell, C. E., Xu, L., Peischl, J., Gilman, J. B., Lamplugh, A., Bowman, H. J., Aikin, K.,  
870 Harkins, C., Zhu, Q., Schwantes, R. H., He, J., Li, M., Seltzer, K., McDonald, B., and Warneke, C.:  
871 Contribution of cooking emissions to the urban volatile organic compounds in Las Vegas, NV, *Atmospheric*  
872 *Chemistry and Physics*, 24, 4289-4304, [10.5194/acp-24-4289-2024](https://doi.org/10.5194/acp-24-4289-2024), 2024a.

873 Coggon, M. M., Stockwell, C. E., Clafin, M. S., Pfannerstill, E. Y., Xu, L., Gilman, J. B., Marcantonio, J., Cao,  
874 C., Bates, K., Gkatzelis, G. I., Lamplugh, A., Katz, E. F., Arata, C., Apel, E. C., Hornbrook, R. S., Piel, F.,  
875 Majluf, F., Blake, D. R., Wisthaler, A., Canagaratna, M., Lerner, B. M., Goldstein, A. H., Mak, J. E., and  
876 Warneke, C.: Identifying and correcting interferences to PTR-ToF-MS measurements of isoprene and other  
877 urban volatile organic compounds, *Atmos. Meas. Tech.*, 17, 801-825, [10.5194/amt-17-801-2024](https://doi.org/10.5194/amt-17-801-2024), 2024b.

878 Crippa, M., DeCarlo, P. F., Slowik, J. G., Mohr, C., Heringa, M. F., Chirico, R., Poulain, L., Freutel, F., Sciare,  
879 J., Cozic, J., Di Marco, C. F., Elsasser, M., Nicolas, J. B., Marchand, N., Abidi, E., Wiedensohler, A.,  
880 Drewnick, F., Schneider, J., Borrmann, S., Nemitz, E., Zimmermann, R., Jaffrezo, J. L., Prévôt, A. S. H., and  
881 Baltensperger, U.: Wintertime aerosol chemical composition and source apportionment of the organic fraction  
882 in the metropolitan area of Paris, *Atmospheric Chemistry and Physics*, 13, 961-981, [10.5194/acp-13-961-2013](https://doi.org/10.5194/acp-13-961-2013),  
883 2013.

884 Daellenbach, K. R., Kourtschev, I., Vogel, A. L., Bruns, E. A., Jiang, J., Petäjä, T., Jaffrezo, J.-L., Aksoyoglu, S.,  
885 Kalberer, M., Baltensperger, U., El Haddad, I., and Prévôt, A. S. H.: Impact of anthropogenic and biogenic  
886 sources on the seasonal variation in the molecular composition of urban organic aerosols: a field and laboratory  
887 study using ultra-high-resolution mass spectrometry, *Atmospheric Chemistry and Physics*, 19, 5973-5991,  
888 [10.5194/acp-19-5973-2019](https://doi.org/10.5194/acp-19-5973-2019), 2019.

889 Debevec, C., Sauvage, S., Gros, V., Salameh, T., Sciare, J., Dulac, F., and Locoge, N.: Seasonal variation and  
890 origins of volatile organic compounds observed during 2 years at a western Mediterranean remote background  
891 site (Ersa, Cape Corsica), *Atmospheric Chemistry and Physics*, 21, 1449-1484, [10.5194/acp-21-1449-2021](https://doi.org/10.5194/acp-21-1449-2021),  
892 2021.

893 Docherty, K. S., Aiken, A. C., Huffman, J. A., Ulbrich, I. M., DeCarlo, P. F., Sueper, D., Worsnop, D. R., Snyder,  
894 D. C., Peltier, R. E., Weber, R. J., Grover, B. D., Eatough, D. J., Williams, B. J., Goldstein, A. H., Ziemann,  
895 P. J., and Jimenez, J. L.: The 2005 Study of Organic Aerosols at Riverside (SOAR-1): instrumental  
896 intercomparisons and fine particle composition, *Atmospheric Chemistry and Physics*, 11, 12387-12420,  
897 [10.5194/acp-11-12387-2011](https://doi.org/10.5194/acp-11-12387-2011), 2011.

898 Eichler, P., Müller, M., D'Anna, B., and Wisthaler, A.: A novel inlet system for online chemical analysis of semi-  
899 volatile submicron particulate matter, *Atmospheric Measurement Techniques*, 8, 1353-1360, 10.5194/amt-8-  
900 1353-2015, 2015.

901 Elser, M., Huang, R.-J., Wolf, R., Slowik, J. G., Wang, Q., Canonaco, F., Li, G., Bozzetti, C., Daellenbach, K. R.,  
902 Huang, Y., Zhang, R., Li, Z., Cao, J., Baltensperger, U., El-Haddad, I., and Prévôt, A. S. H.: New insights into  
903 PM<sub>2.5</sub> chemical composition and sources in two major cities in China during extreme haze events using  
904 aerosol mass spectrometry, *Atmospheric Chemistry and Physics*, 16, 3207-3225, 10.5194/acp-16-3207-2016,  
905 2016.

906 Fleming, L. T., Lin, P., Roberts, J. M., Selimovic, V., Yokelson, R., Laskin, J., Laskin, A., and Nizkorodov, S.  
907 A.: Molecular composition and photochemical lifetimes of brown carbon chromophores in biomass burning  
908 organic aerosol, *Atmospheric Chemistry and Physics*, 20, 1105-1129, 10.5194/acp-20-1105-2020, 2020.

909 Frenay, E. J., Sellegri, K., Canonaco, F., Boulon, J., Hervo, M., Weigel, R., Pichon, J. M., Colomb, A., Prévôt, A.  
910 S. H., and Laj, P.: Seasonal variations in aerosol particle composition at the puy-de-Dôme research station in  
911 France, *Atmospheric Chemistry and Physics*, 11, 13047-13059, 10.5194/acp-11-13047-2011, 2011.

912 Gkatzelis, G. I., Coggon, M. M., McDonald, B. C., Peischl, J., Gilman, J. B., Aikin, K. C., Robinson, M. A.,  
913 Canonaco, F., Prevot, A. S. H., Trainer, M., and Warneke, C.: Observations Confirm that Volatile Chemical  
914 Products Are a Major Source of Petrochemical Emissions in U.S. Cities, *Environ Sci Technol*, 55, 4332-4343,  
915 10.1021/acs.est.0c05471, 2021.

916 Gkatzelis, G. I., Tillmann, R., Hohaus, T., Müller, M., Eichler, P., Xu, K.-M., Schlag, P., Schmitt, S. H., Wegener,  
917 R., Kaminski, M., Holzinger, R., Wisthaler, A., and Kiendler-Scharr, A.: Comparison of three aerosol  
918 chemical characterization techniques utilizing PTR-ToF-MS: a study on freshly formed and aged biogenic  
919 SOA, *Atmospheric Measurement Techniques*, 11, 1481-1500, 10.5194/amt-11-1481-2018, 2018a.

920 Gkatzelis, G. I., Hohaus, T., Tillmann, R., Gensch, I., Müller, M., Eichler, P., Xu, K.-M., Schlag, P., Schmitt, S.  
921 H., Yu, Z., Wegener, R., Kaminski, M., Holzinger, R., Wisthaler, A., and Kiendler-Scharr, A.: Gas-to-particle  
922 partitioning of major biogenic oxidation products: a study on freshly formed and aged biogenic SOA,  
923 *Atmospheric Chemistry and Physics*, 18, 12969-12989, 10.5194/acp-18-12969-2018, 2018b.

924 Grange, S. K., Fischer, A., Zellweger, C., Alastuey, A., Querol, X., Jaffrezo, J.-L., Weber, S., Uzu, G., and Hueglin,  
925 C.: Switzerland's PM<sub>10</sub> and PM<sub>2.5</sub> environmental increments show the importance of non-exhaust emissions,  
926 *Atmospheric Environment: X*, 12, 100145, <https://doi.org/10.1016/j.aeaoa.2021.100145>, 2021.

927 Gruber, R. P. and Kalamas, N.: Current Concepts towards the Health Hazards of BBQ Smoke and Newer  
928 Possibilities for Risk Mitigation: A Pilot Study, *Journal of Biomedical Research & Environmental Sciences*,  
929 5, 675-682, 10.37871/jbres1942, 2024.

930 Guo, J., Zhang, J., Shao, J., Chen, T., Bai, K., Sun, Y., Li, N., Wu, J., Li, R., Li, J., Guo, Q., Cohen, J. B., Zhai,  
931 P., Xu, X., and Hu, F.: A merged continental planetary boundary layer height dataset based on high-resolution  
932 radiosonde measurements, ERA5 reanalysis, and GLDAS, *Earth Syst. Sci. Data*, 16, 1-14, 10.5194/essd-16-  
933 1-2024, 2024.

934 Huang, D. D., Zhu, S., An, J., Wang, Q., Qiao, L., Zhou, M., He, X., Ma, Y., Sun, Y., Huang, C., Yu, J. Z., and  
935 Zhang, Q.: Comparative Assessment of Cooking Emission Contributions to Urban Organic Aerosol Using  
936 Online Molecular Tracers and Aerosol Mass Spectrometry Measurements, *Environ Sci Technol*, 55, 14526-  
937 14535, 10.1021/acs.est.1c03280, 2021.

938 Huang, W., Saathoff, H., Shen, X., Ramisetty, R., Leisner, T., and Mohr, C.: Seasonal characteristics of organic  
939 aerosol chemical composition and volatility in Stuttgart, Germany, *Atmospheric Chemistry and Physics*, 19,  
940 11687-11700, 10.5194/acp-19-11687-2019, 2019.

941 Huang, X.-F., Zou, B.-B., He, L.-Y., Hu, M., Prévôt, A. S. H., and Zhang, Y.-H.: Exploration of PM<sub>2.5</sub> sources on  
942 the regional scale in the Pearl River Delta based on ME-2 modeling, *Atmospheric Chemistry and Physics*, 18,  
943 11563-11580, 10.5194/acp-18-11563-2018, 2018.

944 IPCC: Climate Change 2023: Synthesis Report. Contribution of Working Groups I, II and III to the Sixth  
945 Assessment Report of the Intergovernmental Panel on Climate Change 2023.

946 J. L. Jimenez, M. R. Canagaratna, N. M. Donahue, A. S. H. Prevot, Q. Zhang, J. H. Kroll, P. F. DeCarlo, J. D.  
947 Allan, H. Coe, N. L. Ng, A. C. Aiken, K. S. Docherty, I. M. Ulbrich, and Grieshop, A. P.: Evolution of organic  
948 aerosols in the atmosphere, *Science*, 326, 1525-1529, DOI: 10.1126/science.1180353, 2009.

949 Jain, V., Tripathi, S. N., Tripathi, N., Sahu, L. K., Gaddamidi, S., Shukla, A. K., Bhattu, D., and Ganguly, D.:  
950 Seasonal variability and source apportionment of non-methane VOCs using PTR-TOF-MS measurements in  
951 Delhi, India, *Atmospheric Environment*, 283, 10.1016/j.atmosenv.2022.119163, 2022.

952 Kabir, E., Kim, K. H., Ahn, J. W., Hong, O. F., and Sohn, J. R.: Barbecue charcoal combustion as a potential  
953 source of aromatic volatile organic compounds and carbonyls, *J Hazard Mater*, 174, 492-499,  
954 10.1016/j.jhazmat.2009.09.079, 2010.

955 Kajos, M. K., Rantala, P., Hill, M., Hellén, H., Aalto, J., Patokoski, J., Taipale, R., Hoerger, C. C., Reimann, S.,  
956 and Ruuskanen, T. M.: Ambient measurements of aromatic and oxidized VOCs by PTR-MS and GC-MS:  
957 intercomparison between four instruments in a boreal forest in Finland, *Atmospheric Measurement*  
958 *Techniques*, 8, 4453-4473, 2015.

959 Kim, E., Hopke, P. K., Larson, T. V., Maykut, N. N., and Lewtas, J.: Factor Analysis of Seattle Fine Particles,  
960 *Aerosol Science and Technology*, 38, 724-738, 10.1080/02786820490490119, 2004.

961 Kodros, J. K., Papanastasiou, D. K., Paglione, M., Masiol, M., Squizzato, S., Florou, K., Skyllakou, K.,  
962 Kaltsonoudis, C., Nenes, A., and Pandis, S. N.: Rapid dark aging of biomass burning as an overlooked source  
963 of oxidized organic aerosol, *Proc Natl Acad Sci U S A*, 117, 33028-33033, 10.1073/pnas.2010365117, 2020.

964 Koss, A. R., Sekimoto, K., Gilman, J. B., Selimovic, V., Coggon, M. M., Zarzana, K. J., Yuan, B., Lerner, B. M.,  
965 Brown, S. S., Jimenez, J. L., Krechmer, J., Roberts, J. M., Warneke, C., Yokelson, R. J., and de Gouw, J.:  
966 Non-methane organic gas emissions from biomass burning: identification, quantification, and emission factors  
967 from PTR-ToF during the FIREX 2016 laboratory experiment, *Atmospheric Chemistry and Physics*, 18, 3299-  
968 3319, 10.5194/acp-18-3299-2018, 2018.

969 Kourtchev, I., Godoi, R. H. M., Connors, S., Levine, J. G., Archibald, A. T., Godoi, A. F. L., Paralovo, S. L.,  
970 Barbosa, C. G. G., Souza, R. A. F., Manzi, A. O., Seco, R., Sjostedt, S., Park, J.-H., Guenther, A., Kim, S.,  
971 Smith, J., Martin, S. T., and Kalberer, M.: Molecular composition of organic aerosols in central Amazonia: an  
972 ultra-high-resolution mass spectrometry study, *Atmospheric Chemistry and Physics*, 16, 11899-11913,  
973 10.5194/acp-16-11899-2016, 2016.

974 Kumar, B., Chakraborty, A., Tripathi, S. N., and Bhattu, D.: Highly time resolved chemical characterization of  
975 submicron organic aerosols at a polluted urban location, *Environ Sci Process Impacts*, 18, 1285-1296,  
976 10.1039/c6em00392c, 2016.

977 Kumar, V., Giannoukos, S., Haslett, S. L., Tong, Y., Singh, A., Bertrand, A., Lee, C. P., Wang, D. S., Bhattu, D.,  
978 Stefenelli, G., Dave, J. S., Puthussery, J. V., Qi, L., Vats, P., Rai, P., Casotto, R., Satish, R., Mishra, S.,  
979 Pospisilova, V., Mohr, C., Bell, D. M., Ganguly, D., Verma, V., Rastogi, N., Baltensperger, U., Tripathi, S.  
980 N., Prévôt, A. S. H., and Slowik, J. G.: Highly time-resolved chemical speciation and source apportionment  
981 of organic aerosol components in Delhi, India, using extractive electrospray ionization mass spectrometry,  
982 *Atmospheric Chemistry and Physics*, 22, 7739-7761, 10.5194/acp-22-7739-2022, 2022.

983 Lalchandani, V., Kumar, V., Tobler, A., M. Thamban, N., Mishra, S., Slowik, J. G., Bhattu, D., Rai, P., Satish,  
984 R., Ganguly, D., Tiwari, S., Rastogi, N., Tiwari, S., Močnik, G., Prévôt, A. S. H., and Tripathi, S. N.: Real-  
985 time characterization and source apportionment of fine particulate matter in the Delhi megacity area during  
986 late winter, *Science of The Total Environment*, 770, 10.1016/j.scitotenv.2021.145324, 2021.

987 Lannuque, V., D'Anna, B., Kostenidou, E., Couvidat, F., Martinez-Valiente, A., Eichler, P., Wisthaler, A., Müller,  
988 M., Temime-Roussel, B., Valorso, R., and Sartelet, K.: Gas-particle partitioning of toluene oxidation products:  
989 an experimental and modeling study, *Atmospheric Chemistry and Physics*, 23, 15537-15560, 10.5194/acp-23-  
990 15537-2023, 2023.

991 Leglise, J., Muller, M., Piel, F., Otto, T., and Wisthaler, A.: Bulk Organic Aerosol Analysis by Proton-Transfer-  
992 Reaction Mass Spectrometry: An Improved Methodology for the Determination of Total Organic Mass, O:C  
993 and H:C Elemental Ratios, and the Average Molecular Formula, *Anal Chem*, 91, 12619-12624,  
994 10.1021/acs.analchem.9b02949, 2019.

995 Lemieux, P. M., Lutes, C. C., and Santoianni, D. A.: Emissions of organic air toxics from open burning: a  
996 comprehensive review, *Progress in Energy and Combustion Science*, 30, 1-32, 10.1016/j.peccs.2003.08.001,  
997 2004.

998 Lenssen, E. S., Pieters, R. H. H., Nijmeijer, S. M., Oldenwening, M., Meliefste, K., and Hoek, G.: Short-term  
999 associations between barbecue fumes and respiratory health in young adults, *Environ Res*, 204, 111868,  
1000 10.1016/j.envres.2021.111868, 2022.

1001 Li, H., Riva, M., Rantala, P., Heikkinen, L., Daellenbach, K., Krechmer, J. E., Flaud, P.-M., Worsnop, D., Kulmala,  
1002 M., Villenave, E., Perraudin, E., Ehn, M., and Bianchi, F.: Terpenes and their oxidation products in the French  
1003 Landes forest: insights from Vocus PTR-TOF measurements, *Atmospheric Chemistry and Physics*, 20, 1941-  
1004 1959, 10.5194/acp-20-1941-2020, 2020a.

1005 Li, S., Liu, D., Wu, Y., Hu, K., Jiang, X., Tian, P., Sheng, J., Pan, B., and Zhao, D.: Aging effects on residential  
1006 biomass burning emissions under quasi-real atmospheric conditions, *Environ Pollut*, 337, 122615,  
1007 10.1016/j.envpol.2023.122615, 2023.

1008 Li, W., Wang, J., Qi, L., Yu, W., Nie, D., Shi, S., Gu, C., Ge, X., and Chen, M.: Molecular characterization of  
1009 biomass burning tracer compounds in fine particles in Nanjing, China, *Atmospheric Environment*, 240,  
1010 10.1016/j.atmosenv.2020.117837, 2020b.

1011 Liu, T., Wang, Z., Wang, X., and Chan, C. K.: Primary and secondary organic aerosol from heated cooking oil  
1012 emissions, *Atmospheric Chemistry and Physics*, 18, 11363-11374, 10.5194/acp-18-11363-2018, 2018.

1013 Ma, J., Wang, S., Chen, G., Zhu, S., Wang, P., Chen, J., and Zhang, H.: Estimating emissions of biogenic volatile  
1014 organic compounds from urban green spaces and their contributions to secondary pollution, *Environmental  
1015 Science: Atmospheres*, 5, 129-141, 10.1039/d4ea00099d, 2025.

1016 Maison, A., Lugon, L., Park, S.-J., Baudic, A., Cantrell, C., Couvidat, F., D'Anna, B., Di Biagio, C., Gratien, A.,  
1017 Gros, V., Kalalian, C., Kammer, J., Michoud, V., Petit, J.-E., Shahin, M., Simon, L., Valari, M., Vigneron, J.,  
1018 Tuzet, A., and Sartelet, K.: Significant impact of urban tree biogenic emissions on air quality estimated by a  
1019 bottom-up inventory and chemistry transport modeling, *Atmospheric Chemistry and Physics*, 24, 6011-6046,  
1020 10.5194/acp-24-6011-2024, 2024.

1021 Malik, T. G., Sahu, L. K., Gupta, M., Mir, B. A., Gajbhiye, T., Dubey, R., Clavijo McCormick, A., and Pandey,  
1022 S. K.: Environmental Factors Affecting Monoterpene Emissions from Terrestrial Vegetation, *Plants (Basel)*,  
1023 12, 10.3390/plants12173146, 2023.

1024 Massoli, P., Stark, H., Canagaratna, M. R., Krechmer, J. E., Xu, L., Ng, N. L., Mauldin, R. L., Yan, C., Kimmel,  
1025 J., Misztal, P. K., Jimenez, J. L., Jayne, J. T., and Worsnop, D. R.: Ambient Measurements of Highly Oxidized  
1026 Gas-Phase Molecules during the Southern Oxidant and Aerosol Study (SOAS) 2013, *ACS Earth and Space*  
1027 *Chemistry*, 2, 653-672, 10.1021/acsearthspacechem.8b00028, 2018.

1028 Middlebrook, A. M., Bahreini, R., Jimenez, J. L., and Canagaratna, M. R.: Evaluation of Composition-Dependent  
1029 Collection Efficiencies for the Aerodyne Aerosol Mass Spectrometer using Field Data, *Aerosol Science and*  
1030 *Technology*, 46, 258-271, 10.1080/02786826.2011.620041, 2012.

1031 Molteni, U., Bianchi, F., Klein, F., El Haddad, I., Frege, C., Rossi, M. J., Dommen, J., and Baltensperger, U.:  
1032 Formation of highly oxygenated organic molecules from aromatic compounds, *Atmospheric Chemistry and*  
1033 *Physics*, 18, 1909-1921, 10.5194/acp-18-1909-2018, 2018.

1034 Muller, M., Eichler, P., D'Anna, B., Tan, W., and Wisthaler, A.: Direct Sampling and Analysis of Atmospheric  
1035 Particulate Organic Matter by Proton-Transfer-Reaction Mass Spectrometry, *Anal Chem*, 89, 10889-10897,  
1036 10.1021/acs.analchem.7b02582, 2017.

1037 Müller, M., Mikoviny, T., Jud, W., D'Anna, B., and Wisthaler, A.: A new software tool for the analysis of high  
1038 resolution PTR-TOF mass spectra, *Chemometrics and Intelligent Laboratory Systems*, 127, 158-165,  
1039 10.1016/j.chemolab.2013.06.011, 2013.

1040 München, S.: LHM Stat. Faltkarte, [https://stadt.muenchen.de/dam/jcr%3AAddaedd0e-0914-4093-b46a-  
1041 5a62acc9bf9/LHM-StatTB\\_2023\\_DS.pdf?utm\\_source=chatgpt.com](https://stadt.muenchen.de/dam/jcr%3AAddaedd0e-0914-4093-b46a-5a62acc9bf9/LHM-StatTB_2023_DS.pdf?utm_source=chatgpt.com), 2023.

1042 Nakao, S., Clark, C., Tang, P., Sato, K., and Cocker Iii, D.: Secondary organic aerosol formation from phenolic  
1043 compounds in the absence of NO<sub>x</sub>, *Atmospheric Chemistry and Physics*, 11, 10649-10660, 10.5194/acp-11-  
1044 10649-2011, 2011.

1045 Nault, B. A., Jo, D. S., McDonald, B. C., Campuzano-Jost, P., Day, D. A., Hu, W., Schroder, J. C., Allan, J.,  
1046 Blake, D. R., Canagaratna, M. R., Coe, H., Coggon, M. M., DeCarlo, P. F., Diskin, G. S., Dunmore, R., Flocke,  
1047 F., Fried, A., Gilman, J. B., Gkatzelis, G., Hamilton, J. F., Hanisco, T. F., Hayes, P. L., Henze, D. K., Hodzic,  
1048 A., Hopkins, J., Hu, M., Huey, L. G., Jobson, B. T., Kuster, W. C., Lewis, A., Li, M., Liao, J., Nawaz, M. O.,  
1049 Pollack, I. B., Peischl, J., Rappenglück, B., Reeves, C. E., Richter, D., Roberts, J. M., Ryerson, T. B., Shao,  
1050 M., Sommers, J. M., Walega, J., Warneke, C., Weibring, P., Wolfe, G. M., Young, D. E., Yuan, B., Zhang,  
1051 Q., de Gouw, J. A., and Jimenez, J. L.: Secondary organic aerosols from anthropogenic volatile organic  
1052 compounds contribute substantially to air pollution mortality, *Atmospheric Chemistry and Physics*, 21, 11201-  
1053 11224, 10.5194/acp-21-11201-2021, 2021.

1054 Niu, Y., Yan, Y., Li, J., Liu, P., Liu, Z., Hu, D., Peng, L., and Wu, J.: Establishment and verification of  
1055 anthropogenic volatile organic compound emission inventory in a typical coal resource-based city, *Environ*  
1056 *Pollut*, 288, 117794, 10.1016/j.envpol.2021.117794, 2021.

1057 Ortega, A. M., Day, D. A., Cubison, M. J., Brune, W. H., Bon, D., de Gouw, J. A., and Jimenez, J. L.: Secondary  
1058 organic aerosol formation and primary organic aerosol oxidation from biomass-burning smoke in a flow  
1059 reactor during FLAME-3, *Atmospheric Chemistry and Physics*, 13, 11551-11571, 10.5194/acp-13-11551-  
1060 2013, 2013.

1061 Paatero, P.: The Multilinear Engine—A Table-Driven, Least Squares Program for Solving Multilinear Problems,  
1062 Including then-Way Parallel Factor Analysis Model, *Journal of Computational and Graphical Statistics*, 8,  
1063 854-888, 10.1080/10618600.1999.10474853, 1999.

1064 Paatero, P. and Tapper, U.: Positive matrix factorization: A non-negative factor model with optimal utilization of  
1065 error estimates of data values, *Environmetrics*, 5, 111-126, 10.1002/env.3170050203, 1994.

1066 Peron, A., Graus, M., Striednig, M., Lamprecht, C., Wohlfahrt, G., and Karl, T.: Deciphering anthropogenic and  
1067 biogenic contributions to selected non-methane volatile organic compound emissions in an urban area,  
1068 *Atmospheric Chemistry and Physics*, 24, 7063-7083, 10.5194/acp-24-7063-2024, 2024.

1069 Peter F. DeCarlo, Joel R. Kimmel, Achim Trimborn, Megan J. Northway, John T. Jayne, Allison C. Aiken, Marc  
1070 Gonin, Katrin Fuhrer, Thomas Horvath, Kenneth S. Docherty, Doug R. Worsnop, and Jimenez, J. L.: Field-  
1071 Deployable, High-Resolution, Time-of-Flight Aerosol Mass Spectrometer, *Analytical Chemistry*, 78, 8281-  
1072 8289, 10.1029/2001jd001213, 2006.

1073 Pfannerstill, E. Y., Wang, N., Edtbauer, A., Bourtsoukidis, E., Crowley, J. N., Dienhart, D., Eger, P. G., Ernle, L.,  
1074 Fischer, H., Hottmann, B., Paris, J.-D., Stöner, C., Tadic, I., Walter, D., Lelieveld, J., and Williams, J.:  
1075 Shipborne measurements of total OH reactivity around the Arabian Peninsula and its role in ozone chemistry,  
1076 *Atmospheric Chemistry and Physics*, 19, 11501-11523, 10.5194/acp-19-11501-2019, 2019.

1077 Philippe Dagaut, Zahraa Dbouk , Nesrine Belhadj , Maxence Lailliau , and Benoit, R.: On the combustion of  
1078 terpenes biofuels, *ASME Turbo Expo 2024: Turbomachinery Technical Conference and Exposition*, London,  
1079 United Kingdom, DOI: 10.1115/GT2024-121549, 2024.

1080 Piel, F., Müller, M., Mikoviny, T., Pusede, S. E., and Wisthaler, A.: Airborne measurements of particulate organic  
1081 matter by proton-transfer-reaction mass spectrometry (PTR-MS): a pilot study, *Atmospheric Measurement*  
1082 *Techniques*, 12, 5947-5958, 10.5194/amt-12-5947-2019, 2019.

1083 Pugliese, G., Piel, F., Trefz, P., Sulzer, P., Schubert, J. K., and Miekisch, W.: Effects of modular ion-funnel  
1084 technology onto analysis of breath VOCs by means of real-time mass spectrometry, *Anal Bioanal Chem*, 412,  
1085 7131-7140, 10.1007/s00216-020-02846-8, 2020.

1086 Qadir, R. M., Abbaszade, G., Schnelle-Kreis, J., Chow, J. C., and Zimmermann, R.: Concentrations and source  
1087 contributions of particulate organic matter before and after implementation of a low emission zone in Munich,  
1088 Germany, *Environ Pollut*, 175, 158-167, 10.1016/j.envpol.2013.01.002, 2013.

1089 Qi, L., Vogel, A. L., Esmaeilirad, S., Cao, L., Zheng, J., Jaffrezzo, J.-L., Fermo, P., Kasper-Giebl, A., Daellenbach,  
1090 K. R., Chen, M., Ge, X., Baltensperger, U., Prévôt, A. S. H., and Slowik, J. G.: A 1-year characterization of  
1091 organic aerosol composition and sources using an extractive electrospray ionization time-of-flight mass  
1092 spectrometer (EESI-TOF), *Atmospheric Chemistry and Physics*, 20, 7875-7893, 10.5194/acp-20-7875-2020,  
1093 2020.

1094 Reizer, M., Calzolari, G., Maciejewska, K., Orza, J. A. G., Carraresi, L., Lucarelli, F., and Juda-Rezler, K.:  
1095 Measurement report: Receptor modeling for source identification of urban fine and coarse particulate matter  
1096 using hourly elemental composition, *Atmos. Chem. Phys.*, 21, 14471-14492, 10.5194/acp-21-14471-2021,  
1097 2021.

1098 Ren, Y., Ge, Y., Gu, B., Min, Y., Tani, A., and Chang, J.: Role of management strategies and environmental  
1099 factors in determining the emissions of biogenic volatile organic compounds from urban greenspaces, *Environ*  
1100 *Sci Technol*, 48, 6237-6246, 10.1021/es4054434, 2014.

1101 Renard, J.-B., Becker, G., Nodorft, M., Tavakoli, E., Thiele, L., Poincelet, E., Scholz, M., and Surcin, J.: High-  
1102 Spatial Resolution Maps of PM<sub>2.5</sub> Using Mobile Sensors on Buses: A Case Study of Teltow City, Germany,  
1103 in the Suburb of Berlin, 2023, 10.3390/atmos15121494, 2024.

1104 Resler, J., Baueroová, P., Belda, M., Bureš, M., Eben, K., Fuka, V., Geletič, J., Jareš, R., Karel, J., Keder, J., Krč,  
1105 P., Patiño, W., Radović, J., Řezníček, H., Sührling, M., Šindelářová, A., and Vlček, O.: Challenges of high-  
1106 fidelity air quality modeling in urban environments – PALM sensitivity study during stable conditions,  
1107 *Geoscientific Model Development*, 17, 7513-7537, 10.5194/gmd-17-7513-2024, 2024.

1108 Reyes-Villegas, E., Green, D. C., Priestman, M., Canonaco, F., Coe, H., Prévôt, A. S. H., and Allan, J. D.: Organic  
1109 aerosol source apportionment in London 2013 with ME-2: exploring the solution space with annual and  
1110 seasonal analysis, *Atmospheric Chemistry and Physics*, 16, 15545-15559, 10.5194/acp-16-15545-2016, 2016.

1111 Reyes-Villegas, E., Bannan, T., Le Breton, M., Mehra, A., Priestley, M., Percival, C., Coe, H., and Allan, J. D.:  
1112 Online Chemical Characterization of Food-Cooking Organic Aerosols: Implications for Source  
1113 Apportionment, *Environ Sci Technol*, 52, 5308-5318, 10.1021/acs.est.7b06278, 2018.

1114 Rios, J. C. R.: *Atmospheric Chemistry of Isoprene Hydroxyhydroperoxides*, The Department of Chemistry and  
1115 Chemical Biology, Harvard University, 159 pp., 2018.

1116 Riva, M., Budisulistiorini, S. H., Chen, Y., Zhang, Z., D'Ambro, E. L., Zhang, X., Gold, A., Turpin, B. J., Thornton,  
1117 J. A., Canagaratna, M. R., and Surratt, J. D.: Chemical Characterization of Secondary Organic Aerosol from  
1118 Oxidation of Isoprene Hydroxyhydroperoxides, *Environ Sci Technol*, 50, 9889-9899,  
1119 10.1021/acs.est.6b02511, 2016.

1120 Romanias, M. N., Coggon, M. M., Al Ali, F., Burkholder, J. B., Dagaut, P., Decker, Z., Warneke, C., Stockwell,  
1121 C. E., Roberts, J. M., Tomas, A., Houzel, N., Coeur, C., and Brown, S. S.: Emissions and Atmospheric  
1122 Chemistry of Furanoids from Biomass Burning: Insights from Laboratory to Atmospheric Observations, *ACS*  
1123 *Earth and Space Chemistry*, 8, 857-899, 10.1021/acsearthspacechem.3c00226, 2024.

1124 Samad, A., Caballero Arciénega, N. A., Alabdallah, T., and Vogt, U.: Application of the Urban Climate Model  
1125 PALM-4U to Investigate the Effects of the Diesel Traffic Ban on Air Quality in Stuttgart, *Atmosphere*, 15,  
1126 10.3390/atmos15010111, 2024.

1127 Schäfer, K., Stefan, E., Stefanie, S., Szabina, T., Balint, A., Janos, O., Mike, P., Christoph, Munkel, Josef Cyrus,  
1128 Annette Peters, and Sarigiannis, D.: A measurement based analysis of the spatial distribution, temporal  
1129 variation and chemical composition of particulate matter in Munich and Augsburg, *Int J Tuberc Lung Dis*, 20,  
1130 047-057, 10.5588/ijtld.10.0498, 2011.

1131 Schnell, F. I. J.: *Aerosol distribution above Munich using remote sensing techniques*, Dissertation LMU Munich,  
1132 DOI: 10.5282/edoc.17368, 2014.

1133 Schnelle-Kreis J., Istvan Gebefügi, Gerhard Welzl, Thomas Jaensch, and Kettrup, A.: Occurrence of particle-  
1134 associated polycyclic aromatic compounds in ambient air of the city of Munich, *Atmospheric Environment*,  
1135 35, S71-S81, [https://doi.org/10.1016/S1352-2310\(00\)00557-4](https://doi.org/10.1016/S1352-2310(00)00557-4), 2001.

1136 Seidler, J., Friedrich, M. N., Thomas, C. K., and Nölscher, A. C.: Introducing the novel concept of cumulative  
1137 concentration roses for studying the transport of ultrafine particles from an airport to adjacent residential areas,  
1138 *Atmospheric Chemistry and Physics*, 24, 137-153, 10.5194/acp-24-137-2024, 2024.

1139 Setyan, A., Zhang, Q., Merkel, M., Knighton, W. B., Sun, Y., Song, C., Shilling, J. E., Onasch, T. B., Herndon,  
1140 S. C., Worsnop, D. R., Fast, J. D., Zaveri, R. A., Berg, L. K., Wiedensohler, A., Flowers, B. A., Dubey, M. K.,  
1141 and Subramanian, R.: Characterization of submicron particles influenced by mixed biogenic and  
1142 anthropogenic emissions using high-resolution aerosol mass spectrometry: results from CARES, *Atmospheric*  
1143 *Chemistry and Physics*, 12, 8131-8156, 10.5194/acp-12-8131-2012, 2012.

1144 Song, J., Saathoff, H., Jiang, F., Gao, L., Zhang, H., and Leisner, T.: Sources of organic gases and aerosol particles  
1145 and their roles in nighttime particle growth at a rural forested site in southwest Germany, *Atmospheric*  
1146 *Chemistry and Physics*, 24, 6699-6717, 10.5194/acp-24-6699-2024, 2024.

1147 Song, J., Saathoff, H., Gao, L., Gebhardt, R., Jiang, F., Vallon, M., Bauer, J., Norra, S., and Leisner, T.: Variations  
1148 of PM<sub>2.5</sub> sources in the context of meteorology and seasonality at an urban street canyon in Southwest  
1149 Germany, *Atmospheric Environment*, 282, 10.1016/j.atmosenv.2022.119147, 2022.

1150 Squires, F. A., Nemitz, E., Langford, B., Wild, O., Drysdale, W. S., Acton, W. J. F., Fu, P., Grimmond, C. S. B.,  
1151 Hamilton, J. F., Hewitt, C. N., Hollaway, M., Kotthaus, S., Lee, J., Metzger, S., Pingingtha-Durden, N., Shaw,  
1152 M., Vaughan, A. R., Wang, X., Wu, R., Zhang, Q., and Zhang, Y.: Measurements of traffic-dominated  
1153 pollutant emissions in a Chinese megacity, *Atmospheric Chemistry and Physics*, 20, 8737-8761, 10.5194/acp-  
1154 20-8737-2020, 2020.

1155 Srivastava, D., Vu, T. V., Tong, S., Shi, Z., and Harrison, R. M.: Formation of secondary organic aerosols from  
1156 anthropogenic precursors in laboratory studies, *npj Climate and Atmospheric Science*, 5, 10.1038/s41612-022-  
1157 00238-6, 2022.

1158 Stein, A. F., Draxler, R. R., Rolph, G. D., Stunder, B. J. B., Cohen, M. D., and Ngan, F.: NOAA's HYSPLIT  
1159 Atmospheric Transport and Dispersion Modeling System, *Bulletin of the American Meteorological Society*,  
1160 96, 2059-2077, <https://doi.org/10.1175/BAMS-D-14-00110.1>, 2015.

1161 Stirnberg, R., Cermak, J., Kotthaus, S., Haeffelin, M., Andersen, H., Fuchs, J., Kim, M., Petit, J.-E., and Favez,  
1162 O.: Meteorology-driven variability of air pollution (PM<sub>1</sub>) revealed with explainable machine learning,  
1163 *Atmospheric Chemistry and Physics*, 21, 3919-3948, 10.5194/acp-21-3919-2021, 2021.

1164 Ulbrich, I. M., Canagaratna, M. R., Zhang, Q., Worsnop, D. R., and Jimenez, J. L.: Interpretation of organic  
1165 components from Positive Matrix Factorization of aerosol mass spectrometric data, *Atmos. Chem. Phys.*, 9,  
1166 2891-2918, 10.5194/acp-9-2891-2009, 2009.

1167 Vicente, E. D., Vicente, A., Evtuyugina, M., Carvalho, R., Tarelho, L. A. C., Oduber, F. I., and Alves, C.:  
1168 Particulate and gaseous emissions from charcoal combustion in barbecue grills, *Fuel Processing Technology*,  
1169 176, 296-306, 10.1016/j.fuproc.2018.03.004, 2018.

1170 Wan, X., Kawamura, K., Ram, K., Kang, S., Loewen, M., Gao, S., Wu, G., Fu, P., Zhang, Y., Bhattarai, H., and  
1171 Cong, Z.: Aromatic acids as biomass-burning tracers in atmospheric aerosols and ice cores: A review, *Environ*  
1172 *Pollut*, 247, 216-228, 10.1016/j.envpol.2019.01.028, 2019.

1173 Wang, H., Li, Y., Liu, Y., Lu, X., Zhang, Y., Fan, Q., Shen, C., Lai, S., Zhou, Y., Zhang, T., and Yue, D.:  
1174 Underappreciated contributions of biogenic volatile organic compounds from urban green spaces to ozone  
1175 pollution, *Atmospheric Chemistry and Physics*, 25, 5233-5250, 10.5194/acp-25-5233-2025, 2025.

1176 Wang, L., Slowik, J. G., Tripathi, N., Bhattu, D., Rai, P., Kumar, V., Vats, P., Satish, R., Baltensperger, U.,  
1177 Ganguly, D., Rastogi, N., Sahu, L. K., Tripathi, S. N., and Prévôt, A. S. H.: Source characterization of volatile  
1178 organic compounds measured by proton-transfer-reaction time-of-flight mass spectrometers in Delhi, India,  
1179 *Atmospheric Chemistry and Physics*, 20, 9753-9770, 10.5194/acp-20-9753-2020, 2020a.

1180 Wang, Q., He, X., Zhou, M., Huang, D. D., Qiao, L., Zhu, S., Ma, Y.-g., Wang, H.-l., Li, L., Huang, C., Huang,  
1181 X. H. H., Xu, W., Worsnop, D., Goldstein, A. H., Guo, H., and Yu, J. Z.: Hourly Measurements of Organic  
1182 Molecular Markers in Urban Shanghai, China: Primary Organic Aerosol Source Identification and  
1183 Observation of Cooking Aerosol Aging, *ACS Earth and Space Chemistry*, 4, 1670-1685,  
1184 10.1021/acsearthspacechem.0c00205, 2020b.

1185 Wang, W., Zhang, Y., Jiang, B., Chen, Y., Song, Y., Tang, Y., Dong, C., and Cai, Z.: Molecular characterization  
1186 of organic aerosols in Taiyuan, China: Seasonal variation and source identification, *Sci Total Environ*, 800,  
1187 149419, 10.1016/j.scitotenv.2021.149419, 2021.

1188 Wang, Z., Wang, Z., Sun, J., Wang, Y., Sun, Z., Ma, K., and Wei, L.: Investigation of oxygen-enriched atmosphere  
1189 combustion of oily sludge: Performance, mechanism, emission of the S/N-containing compound, and residue  
1190 characteristics, *Journal of Cleaner Production*, 378, 10.1016/j.jclepro.2022.134233, 2022.

1191 Wenzel, A., Chen, J., Klama, T., Böhm, F., Angleitner, M., and Lobmaier, R.: Towards high-resolution air  
1192 pollutants sensing through dense low-cost sensor networks – a case study in Munich, EGU General Assembly  
1193 2025, Vienna, Austria, 27 Apr–2 May 2025, <https://doi.org/10.5194/egusphere-egu25-16784>,

1194 Williams, L. R., Gonzalez, L. A., Peck, J., Trimborn, D., McInnis, J., Farrar, M. R., Moore, K. D., Jayne, J. T.,  
1195 Robinson, W. A., Lewis, D. K., Onasch, T. B., Canagaratna, M. R., Trimborn, A., Timko, M. T., Magoon, G.,  
1196 Deng, R., Tang, D., de la Rosa Blanco, E., Prévôt, A. S. H., Smith, K. A., and Worsnop, D. R.: Characterization  
1197 of an aerodynamic lens for transmitting particles greater than 1 micrometer in diameter into the Aerodyne  
1198 aerosol mass spectrometer, *Atmospheric Measurement Techniques*, 6, 3271-3280, 10.5194/amt-6-3271-2013,  
1199 2013.

1200 The new 2021 WHO air quality guideline limits. Breeze Technologies Blog: [https://www.breeze-](https://www.breeze-technologies.de/blog/new-2021-who-air-quality-guideline-limits/)  
1201 [technologies.de/blog/new-2021-who-air-quality-guideline-limits/](https://www.breeze-technologies.de/blog/new-2021-who-air-quality-guideline-limits/), last access: November 12.

1202 Wu, C., Wang, C., Wang, S., Wang, W., Yuan, B., Qi, J., Wang, B., Wang, H., Wang, C., Song, W., Wang, X.,  
1203 Hu, W., Lou, S., Ye, C., Peng, Y., Wang, Z., Huangfu, Y., Xie, Y., Zhu, M., Zheng, J., Wang, X., Jiang, B.,  
1204 Zhang, Z., and Shao, M.: Measurement report: Important contributions of oxygenated compounds to emissions  
1205 and chemistry of volatile organic compounds in urban air, *Atmospheric Chemistry and Physics*, 20, 14769-  
1206 14785, 10.5194/acp-20-14769-2020, 2020.

1207 Wu, T., Müller, T., Wang, N., Byron, J., Langer, S., Williams, J., and Licina, D.: Indoor Emission, Oxidation, and  
1208 New Particle Formation of Personal Care Product Related Volatile Organic Compounds, *Environmental*  
1209 *Science & Technology Letters*, 11, 1053-1061, 10.1021/acs.estlett.4c00353, 2024.

1210 Xu, C., Chen, J., Zhang, X., Cai, K., Chen, C., and Xu, B.: Emission characteristics and quantitative assessment  
1211 of the health risks of cooking fumes during outdoor barbecuing, *Environ Pollut*, 323, 121319,  
1212 10.1016/j.envpol.2023.121319, 2023.

1213 Ye, Q., Krechmer, J. E., Shutter, J. D., Barber, V. P., Li, Y., Helstrom, E., Franco, L. J., Cox, J. L., Hrdina, A. I.  
1214 H., Goss, M. B., Tahsini, N., Canagaratna, M., Keutsch, F. N., and Kroll, J. H.: Real-Time Laboratory  
1215 Measurements of VOC Emissions, Removal Rates, and Byproduct Formation from Consumer-Grade  
1216 Oxidation-Based Air Cleaners, *Environmental Science & Technology Letters*, 8, 1020-1025,  
1217 10.1021/acs.estlett.1c00773, 2021.

1218 Yee, L. D., Kautzman, K. E., Loza, C. L., Schilling, K. A., Coggon, M. M., Chhabra, P. S., Chan, M. N., Chan,  
1219 A. W. H., Hersey, S. P., Crounse, J. D., Wennberg, P. O., Flagan, R. C., and Seinfeld, J. H.: Secondary organic  
1220 aerosol formation from biomass burning intermediates: phenol and methoxyphenols, *Atmospheric Chemistry  
1221 and Physics*, 13, 8019-8043, 10.5194/acp-13-8019-2013, 2013.

1222 Yeoman, A. M., Shaw, M., Carslaw, N., Murrells, T., Passant, N., and Lewis, A. C.: Simplified speciation and  
1223 atmospheric volatile organic compound emission rates from non-aerosol personal care products, *Indoor Air*,  
1224 30, 459-472, 10.1111/ina.12652, 2020.

1225 Zhang, H., Huang, W., Shen, X., Ramisetty, R., Song, J., Kiseleva, O., Holst, C. C., Khan, B., Leisner, T., and  
1226 Saathoff, H.: Aerosol composition, air quality, and boundary layer dynamics in the urban background of  
1227 Stuttgart in winter, *Atmospheric Chemistry and Physics*, 24, 10617-10637, 10.5194/acp-24-10617-2024, 2024.

1228 Zhang, Q., Jimenez JI Fau - Canagaratna, M. R., Canagaratna Mr Fau - Ulbrich, I. M., Ulbrich Im Fau - Ng, N.  
1229 L., Ng NI Fau - Worsnop, D. R., Worsnop Dr Fau - Sun, Y., and Sun, Y.: Understanding atmospheric organic  
1230 aerosols via factor analysis of aerosol mass spectrometry: a review, *Anal Bioanal Chem*, 401(10), 3045-3067,  
1231 10.1007/s00216-011-5355-y, 2011.

1232 Zhu, Q., Huang, X.-F., Cao, L.-M., Wei, L.-T., Zhang, B., He, L.-Y., Elser, M., Canonaco, F., Slowik, J. G.,  
1233 Bozzetti, C., El-Haddad, I., and Prévôt, A. S. H.: Improved source apportionment of organic aerosols in  
1234 complex urban air pollution using the multilinear engine (ME-2), *Atmospheric Measurement Techniques*, 11,  
1235 1049-1060, 10.5194/amt-11-1049-2018, 2018.

1236